

EFFECT OF NOZZLE LENGTH AND DIAMETER ON PLUME STABILITY AND NOISE
IN DIRECT CONTACT CONDENSATION OF STEAM IN A SUBCOOLED
CROSSFLOW OF WATER

by
Eli Luis Gaeta

A thesis submitted in partial fulfillment of
the requirements for the degree of

Master of Science
(Mechanical Engineering)

at the
UNIVERSITY OF WISCONSIN-MADISON
2024

Date of final oral examination: December 16, 2024

The dissertation is approved by the following members of the Defense Committee:
Allison J. Mahvi, Assistant Professor, Mechanical Engineering
Arganthaël Berson, Assistant Teaching Professor, Mechanical Engineering
Gregory F. Nellis, William A. and Irene Ouweneel-Bascom Professor, Mechanical
Engineering

© Copyright by Eli Gaeta

ALL RIGHTS RESERVED

Dedicated to Evelyn Parisot

1927-2024

Acknowledgements

The unbelievable support I have received throughout my journey in this life has meant the world to me. I would not be a fraction of the person I am without the unconditional love from my family, friends, and colleagues.

I would first like to thank my committee – Allison Mahvi, Arganthaël Berson, and Greg Nellis – for their expert guidance and steady encouragement throughout my time in Madison. Each of them has been critical to my growth as an engineer. I am especially grateful to Allison for her mentorship, patience, and ability to challenge me to achieve more than I thought possible. I would also like to thank Arganthaël for his curiosity and his wealth of innovative ideas, which provided valuable perspectives in every challenge faced.

Next, I would like to thank my colleagues in the in the LET+S lab-- Jack, Joe, and Payton- - for their friendship, technical support, and humor. To our past alumni—Jason, Roman, and Christian—I am deeply grateful for the warm welcome I received upon joining the lab and for your invaluable guidance on conducting research. The contributions of the undergraduate students who joined this project—Connor, Vaidehi, and Taisir—have been immensely valuable and truly deserving of recognition.

I am deeply grateful for the support from Jim Zaiser and the entire team at Hydro-Thermal Corp. Their willingness to match our curiosity in every aspect of this project has been a constant source of motivation for me.

Each of my teachers and professor throughout my academic career deserves infinite praise for their impact. Thanks for cultivating my curiosity and growth as a person. To Doc Schneider, thank you for being the best role model I could have ever asked for, the love you give to all you

encounter has been the greatest inspiration. To Jim Boudro, thank you for pushing me when I was content, encouraging me to strive for more and reach my fullest potential. Without the encouragement from my teachers at ISU--Michael Messman, Travis Grager, Ganesh Rajagopalan, Carolyn Riedel, Howard Shapiro, Mark Bryden, and Margaret Mathison-- I would not even be in graduate school, thank you for your belief in me. To each of my mentors through my various work experiences; Erin Berry, Jessie McMasters, Dylan Muckey, Jerome Norris, and Evan Dudley, thank you for your excellent leadership, mentorship, and advice.

Finally, to my family, thank you for loving me and supporting me through all seasons of life. Each moment together has been a blessing that I will always cherish. To Sophia, thank you for your unwavering support and love. Most of all, to my mother—your love has guided me through everything I have ever experienced in life. Without your bravery, wisdom, kindness, and compassion I would be nothing. To you I owe everything that I am, was, and will be. Thank you for being you.

Abstract

Direct Contact Condensation (DCC) transfers heat to a process fluid by directly injecting a high-pressure vapor into a subcooled liquid stream. Direct contact condensers have a smaller overall footprint compared to traditional heat exchangers and are used in several industries, including milk pasteurization, emergency cool-down in nuclear power plants, and wastewater treatment. During DCC, vapor is accelerated through small nozzles that generate vapor plumes that penetrate the process fluid. Under certain conditions, the vapor plume becomes unstable and can generate significant noise and vibrations. The goal of this study is to understand the effect of nozzle geometry on plume stability and noise when steam is injected into a crossflow water stream. In these experiments, we characterize the steam plume flow regime and noise level through single- and two-port nozzles. The results quantify the impact of water temperature (25 - 80°C), pressure ratio (0.47 and 0.58), nozzle diameter (1.65 – 3.18 mm), and the nozzle length-to-diameter ratio (1 – 8). This study shows that nozzles with a smaller diameter and smaller length-to-diameter ratio produce less noise and that two smaller holes can have the same mass flow rate (and heating) as one larger nozzle, but less noise.

Thesis Organization

The main body of this thesis contains a journal article that will be submitted in early 2025. I am the first author on this paper and drove the research effort. Christian Thorpe and Madeline Morrell are co-authors on the paper and conducted preliminary testing and analysis on the length to diameter ratio and diameter studies before they graduated in 2023. Although their preliminary findings helped drive our research questions, their data was not used to generate the results. All experimental data was retaken with changes to the measurement methods and reanalyzed using a MATLAB script I generated. All initial single-port nozzles were procured by Christian. I procured a new set of the smallest diameter single-port nozzles ($D = 1.65$ mm and 2.03 mm) discussed in section 3.2 and all dual-port nozzles discussed in section 3.3.

The chapters presented in this thesis detail a comprehensive study of the effects of nozzle length, diameter, and mass flow rate on steam plume stability and noise. Facility upgrades are documented in the appendices. Appendix A provides up-to-date work instructions for running the steam injection facility. Appendix B provides geometric information for the nozzles used in this work. Appendix C describes improvements to the lighting and imaging of the steam plume. The extensive enhancements to the deaeration process are detailed in Appendix D. Improvements to temperature control in the test section are described in Appendix E. Appendix F describes changes to the superheating system. Major plumbing upgrades, including the replacement of rusted and leaking fittings, are documented in Appendix G. Finally, Appendix H explains how to process testing data into plots for analysis and interpretation.

Table of Contents

Acknowledgements.....	ii
Abstract.....	iv
Thesis Organization	v
Table of Contents	vi
List of Tables.....	viii
List of Figures.....	ix
Chapter 1: Introduction.....	1
Chapter 2: Methods.....	5
2.1 Experimental Facility.....	5
2.2 Test Section.....	8
2.3 Flow Regime Characterization	10
Chapter 3: Results and Discussion.....	13
3.1 Effect of Length to Diameter (L/D) Ratio	13
3.2 Effect of Diameter.....	15
3.3 Effect of Mass Flow Rate on Noise Level	17
Chapter 4: Conclusion.....	21
References.....	22
Appendix A: Loop Startup/Operation Instructions.....	24
A.1 Safety	24
A.2 Emergency shutdown.....	24
A.3 Start-up.....	25
A.4 De-aerate the Loop.....	32
A.5 Prep the Camera	35
A.6 Prep the Steam	38
A.7 Collect Data.....	39
A.8 Collecting reference pictures	45
A.9 Loop Shutdown	47
A.10 How to convert cine files to tiff for image processing.....	48
Appendix B: Nozzle Geometry and Scans.....	51
Appendix C: Lighting and Imaging Changes	55
Appendix D: Deaeration Procedure Overhaul	61

Appendix E: Chilled Water Needle Valve Improvements.....	68
Appendix F: Steam Superheating Changes.....	72
F.1 Replacing the Rope Heaters	72
F.2 Replacing the Steam Temperature Measurement.....	75
Appendix G: Rusted Fitting.....	78
Appendix H: Data Organization	82
H.1 How to use NozzleRegimeData Excel Sheet	82
H.2 How to use AnalysisFinal.m	85
H.3 How to use StudyAnalysis.m.....	86

List of Tables

Table 1 Facility Instrumentation	8
Table 2 Nozzle Geometry	10
Table B1 Length to Diameter Nozzles	51
Table B2 Diameter Study Nozzles	52
Table B3 Dual-port Nozzles.....	54
Table E1 Hanbay Needle Valve Wiring Guide.....	69

List of Figures

Figure 1 Steam Injection Facility Diagram.....	6
Figure 2 Test Section Schematic.....	9
Figure 3 Flow Regime Sample Images.....	12
Figure 4 Length to Diameter Ratio Study Flow Regime and Noise Level.....	15
Figure 5 Diameter Study Flow Regime and Noise Level.....	17
Figure 6 Study wide mass flow rate.....	18
Figure 7 Dual-port Study Noise Level.....	20
Figure A1 DAQ Extension Cord Location.....	25
Figure A2 Bladder Tank Scale	26
Figure A3 Various Valve Locations	27
Figure A4 “The_boss” File Location	28
Figure A5 Front Panel of “The_boss”.....	28
Figure A6 R8080 Front Panel	29
Figure A7 “The_boss” Offset Tab.....	29
Figure A8 PCC Front Panel	36
Figure A9 PCC Manager Tab.....	36
Figure A10 PCC CSR Setting.....	37
Figure A11 “The_boss” Front Panel Legend	42
Figure A12 “The_boss” File Saving Panel	43
Figure A13 Data Saving Button Location.....	44
Figure A14 Cine Frame Range Saving	44
Figure A15 PCC File Save Options	46
Figure A16 PCC Batch Convert.....	49
Figure A17 PCC Batch Convert Save Menu.....	49
Figure C1 Front-lit Sample Steam Plume.....	55
Figure C2 Front-lit Sample Reference Image.....	56
Figure C3 Sound Level Meter Mounting Arm.....	57

Figure C4 Lighting and Imaging Evolution..... 58

Figure C5 Current Steam Plume Imagery Sample..... 59

Figure C6 Phantom Camera Optical Tray..... 60

Figure C7 Current Reference Image Sample 60

Figure D1 Steam Injection Loop Diagram from April 2023..... 61

Figure D2 Steam Injection Loop Diagram w/ 4-way Valve 62

Figure D3 Deaeration Valve Manifold..... 63

Figure D4 Air Separator Units 64

Figure F1 Original Rope Heaters 72

Figure F2 VARIAC Superheater Control Unit..... **Error! Bookmark not defined.**

Figure F3 Current Rope Heaters 74

Figure F4 Superheater Insulation Post-install..... 75

Figure F5 Steam Measurement Adjustment w/ Tee 76

Figure F6 Steam Measurement Adjustment w/ Cross 77

Figure G1 Rusted Tee 78

Figure G2 Corroded Heated Steam Length 79

Figure G3 Steam Pressure Regulator..... 79

Figure G4 Rusted Tee Replacement..... 80

Figure G5 Replaced Heated Steam Length..... 81

Figure G6 Replaced Steam Pressure Regulator 81

Figure H1 Nozzle Regime Data Cols. A-Q..... 83

Figure H2 Nozzle Regime Data Cols. R-Z 84

Figure H3 Nozzle Regime Data Cols. X-AB..... 84

Figure H4 AnalysisFinal User Input 85

Figure H5 StudyAnalysis User Input..... 86

Figure H6 Study Analysis Pop Up Window 87

Chapter 1: Introduction

Direct Contact Condensation (DCC) is a heat transfer process in which vapor directly condenses into a liquid stream or tank, releasing its heat of vaporization. Unlike traditional condensers, DCC eliminates the need for a separating wall, enabling direct interaction between the vapor and liquid phases. This direct interaction results in complete energy transfer from the vapor to the liquid, enhancing heat exchange efficiency. DCC is used in a variety of applications, from steaming milk for coffee to industrial processes such as: nuclear reactor cooling during loss-of-coolant accidents, milk pasteurization, municipal wastewater treatment, and pulp washing in the paper industry.

Despite its many advantages, DCC can produce large pressure oscillations and thus high noise levels. The highest noise levels are associated with an instability of the steam plume which leads to large oscillations in the position of the liquid-vapor interface.¹ Understanding the factors influencing plume stability and noise generation is crucial, as the resulting vibrations can lead to mechanical fatigue in industrial equipment over time. Steam plumes can be classified into different regimes based on temporal changes to their shape. Although many authors have categorized plumes into distinct regimes, the literature has been inconsistent in its naming conventions.²

Terms such as condensation oscillation I and II, bubbling, conical jet, ellipsoidal jet, and chugging, among others, have been used for steam plume classification.² Efforts have been made to standardize regime naming by both Zhao et al.³ and Alden et al.² In this work, the simplified four-regime convention proposed by Alden et al. is adopted, as it aligns with the regimes observed in these experiments. These regimes include stable, condensation oscillation, transition, and unstable. As implied by its name, a stable condensing jet has a constant shape with very few width perturbations. When the condensation potential (the temperature difference between the vapor and

liquid)⁴ is lowered, the jet enters the condensation oscillation regime, where instabilities at the vapor-liquid interface result in higher amplitude variations in the plume width and height. Increasing the process fluid temperature further will eventually yield an unstable steam plume. In this regime, high amplitude oscillations in the plume width cause large vapor bubbles to fully detach from the main steam plume. These bubbles then collapse and reform rapidly as they condense.² The transition regime lies between the unstable and condensation oscillation regimes. As a hybrid of the two neighboring states, transitioning plumes flip back and forth between the condensation oscillation and unstable regimes.

The differences in flow patterns have been attributed to surface instabilities.⁵⁻⁷ The source of these instabilities has not been decisively determined. Some groups argue that the instabilities are the result of velocity shear between the two phases (Kelvin-Helmholtz instability)⁶, while other groups argue that they arise from density differences between the vapor and liquid (Rayleigh-Taylor instability)⁷. Either way, surface instabilities cause the steam plume width to oscillate. If the instability causes large amplitude oscillations, discrete bubbles start to form, and the plume will transition into an unstable flow regime. Building on this, Sanaullah et al.⁵ experimentally explored how different levels of subcooling in the process water affected the growth of instabilities, which were attributed to the radial and axial perturbations of the plume. Their key finding was that increased subcooling significantly attenuated instabilities, thus reducing pressure oscillations.

To illustrate how process conditions, including condensation driving potential, influence surface instabilities and flow regimes, several groups have developed DCC flow regime maps. These maps usually predict regime using steam mass flux, process water temperature, pressure ratio, and for flowing process fluid cases—Reynolds number.⁸⁻¹⁰ Most of these maps show that higher process fluid temperatures and higher pressure ratios result in unstable plumes, but there is

some disagreement on the impacts of steam mass flux and Reynolds number. Early investigations focused solely on process fluid temperature (or subcooling) and steam mass flux and showed that higher steam mass fluxes led to increased plume stability^{11,12}. However, subsequent work has shown that these parameters alone are insufficient for predicting DCC flow regimes, especially in crossflow configurations. For example, Alden et al. demonstrated that steam plumes generated with different pressure ratios, but the same mass flux, can be in vastly different regimes. Their proposed maps instead use pressure ratio and degree of subcooling to distinguish regime regions.² Similarly, some authors have shown that increasing the process fluid Reynolds number in crossflow DCC leads to slight improvements in stability¹¹, but others have shown no impact on the process fluid flow rate^{2,10}.

The second main area of study in DCC literature focuses on characterizing pressure oscillations during condensation. Several studies^{1,2,10} demonstrate that oscillations in the plume radius and penetration length are directly correlated to noise generation. The amplitude and frequency of this noise is dependent on the steam plume flow regime.² Cho et al.¹² observed a peak amplitude between 50°C and 80°C, where the steam plumes tend to be in the transition or fully unstable flow regime. Both the unstable and transition regimes have very high amplitude pressure oscillations due to bubble separation and collapse. When the plume is stable, the steam water interface is relatively smooth and has low amplitude pressure oscillations.² During condensation oscillation, the amplitude of the pressure oscillations rise and the dominant frequency lowers compared to the stable regime.

Most authors test a single nozzle geometry^{10,12,13}, and therefore there is little directly comparable information in the literature on the impact of nozzle geometry on flow regime and noise. Some authors have evaluated nozzles with different length to diameter ratios^{14,15}, but

focused on stable condensing jets and did not explicitly study flow regimes or noise. Thorpe et al. evaluated six different nozzles – three converging/converging-diverging nozzles with different area ratios and three straight nozzles with the same base geometry but different small manufacturing defects. They showed that geometry has a large impact on flow regime, and that even relatively small geometric features (burrs or slight chamfers), can significantly impact nozzle performance by affecting the velocity of steam at the exit.⁸ A study by Quddus et al. studied the impact of bevels at the nozzle exit on the steam plume shape. The authors found decreased plume stability with larger bevel angles.¹⁶ Chong et al. varied straight nozzle diameter in a pool injection case, but only observed variations of the unstable regime.¹⁷ To the present authors' knowledge, this work is the first to investigate the effect varying straight nozzle length and diameter has on noise level in cross flow DCC.

The objective of this paper is to evaluate the role of length, diameter, and mass flow rate in straight nozzles on plume stability and noise levels across a range of pressure ratios and process fluid temperatures. This aligns our work with the broader category of research on pressure oscillations and flow regime mapping. Additionally, the study investigates the effect of mass flow rate on overall noise, aiming to determine whether a single larger nozzle or two smaller nozzles with equal total area and mass flux perform better in terms of noise reduction. The experimental work is conducted using a crossflow setup and plume flow regimes are classified through visual inspection of high-speed videos. The results demonstrate that short-length, multiport, small-diameter nozzles should be the design target for applications where noise is a concern. This work provides DCC nozzle designers with comprehensive insights into the geometric design parameters needed for developing effective steam injection heaters.

Chapter 2: Methods

2.1 Experimental Facility

The experimental facility in use for this study is shown in Fig. 1 and is similar to the facility used by Alden et al.² and Thorpe et al.⁸ The purpose of the facility is to condition a process fluid (subcooled water) and steam for direct contact condensation in a crossflowing orientation. The process fluid is pumped using a centrifugal pump (Bell & Gosset 90-4T, maximum flow rate of 75.7 L/min) and the flow rate is controlled using an inline ball valve and is measured using an electromagnetic flowmeter (Toshiba GF630/LF610). For all tests in this study, the flow rate is set to 56.78 L/min (15 gal/min). Prior work has shown that the process fluid flow rate does not significantly impact the steam injection characteristics.² The process fluid then passes through a flow straightener and enters the test section, which is shown in the inset in Figure 1. After the process fluid exits the test section, it is cooled by a heat exchanger coupled to the building chilled water system. A needle valve controls the process fluid temperature at the exit of this heat exchanger by modulating the chilled water flow rate. After the process fluid is cooled, non-condensable gases are passively removed using an air separator (Spirotherm VJR125TM). Finally, the fluid returns to the pump and begins the cycle again. The process fluid pressure (measured using SSI Technologies P51-100-G) is controlled using a pressure control valve and a laboratory compressed air line connected to the top of the bladder tank shown in Fig. 1. In this study, the water pressure is adjusted between runs to achieve the desired pressure ratio across the steam injector. The process fluid pressure was used to set the pressure ratio to eliminate differences in the steam inlet density, which would change the steam mass flow rate at different pressure ratios.

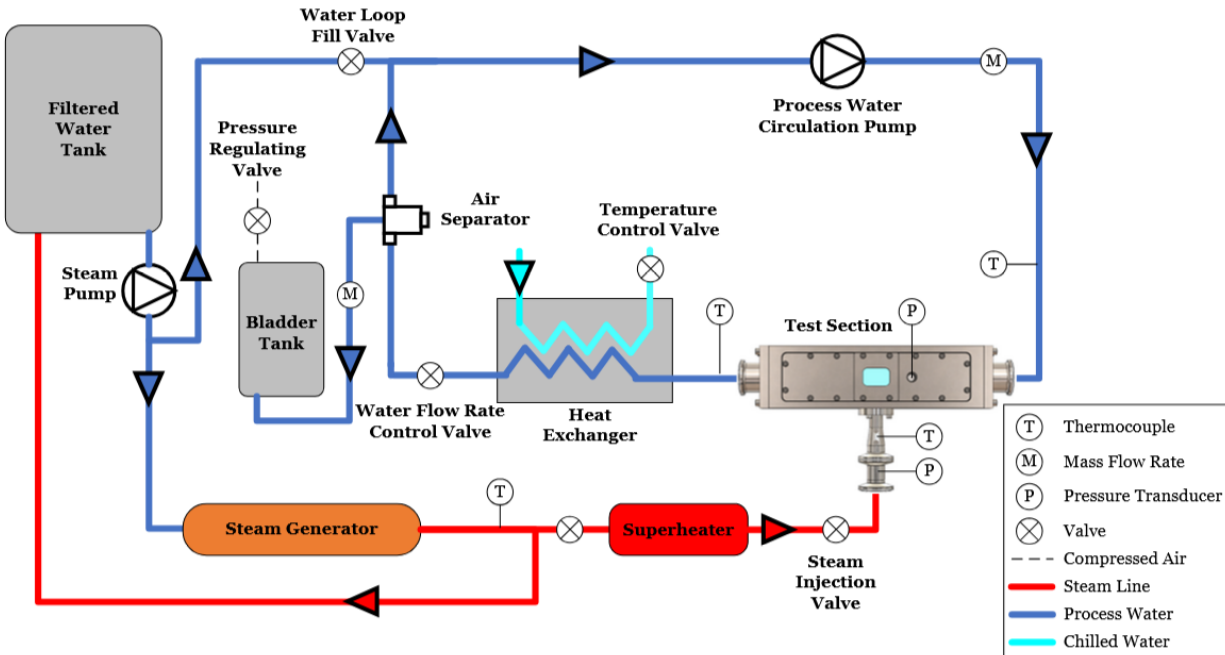


Figure 1: Schematic of the steam injection facility.

Steam is conditioned in a separate steam line and is then injected into the test section through nozzles of varying geometries. The steam line is fed by a 13-gallon water reservoir. First, the water passes into a 48-kW electric boiler (Infinity Fluids, CRES-SG-48-0480-K-3P). A PID system controls the boiler temperature, and since the outlet steam is saturated, the controller ultimately adjusts the steam pressure, which is kept at 483 kPa (70 psig) for all the data shown here. Next, the steam is heated by an electric resistance rope heater (HTS/Amptek AWH-051-080D), which is controlled with a portable transformer (Staco Energy 3PN1010B) to maintain 1-2°C of superheat at the inlet of the test section. Steam temperature and pressure are measured at the inlet of the test section using a type-T thermocouple and a piezoresistive pressure sensor (Baumer PMBH-24H23), respectively. After the steam is injected through the nozzle, steam mass flow rate is measured using a Coriolis flow meter (Emerson CMF010M) at the entrance to the bladder tank, which collects excess mass added to the process fluid by the steam line.

During injection, we record the steam flow pattern and measure the acoustic noise near the test section. A 7,000 lumen LED light (GS Vitec QX Mini) provides backlighting at the test section. A high-speed camera (Phantom v311) with a Nikon Micro-NIKKOR 55mm lens is used to capture and analyze the steam plume flow pattern. The camera is positioned in front of the front quartz window and is initially focused on the steam plume. The camera is then moved via an optical tray to focus on a calibrated target behind the plume to determine the size of each pixel. Once it is calibrated, the camera is moved back to its initial position before data collection begins. All videos are 1 second in duration and are taken at a frame rate of 40,000 fps, a resolution of 256x256 pixels, and an exposure time of 1 μ s. The noise level is measured using a Type 2 sound level meter (REED 8080), which is positioned 1 meter from the test section. This microphone measures the total sound level according to OSHA standard 1910.95 at a sample rate of 2 Hz for 10 seconds.

During each run, we collect 12 data points at process water temperatures between 25 and 80°C. Data is taken at steady state conditions defined as $\pm 0.5^\circ\text{C}$ of the target temperature. All fluid measurements are recorded with a National Instruments data acquisition system (cDAQ-9178) at 1 kHz for 60 seconds. A summary of all the instrumentation used in this experiment is provided in Table 1.

Table 1: Details of instrumentation in facility.

Measurement	Sensor	Location	Span and Uncertainty
Water volumetric flow rate	Toshiba GF630/LF610	Water pump exit	0 to 15 m ³ /hr ± 0.2% of rate
Water pressure	SSI Technologies P51-100-G	Test section water inlet	0 to 690 kPa ± 6.9 kPa
Water temperature	Type-E thermocouple	Various locations	-200 to 900°C ± 1.7°C
Steam mass flow rate	Emerson CMF010M	Bladder tank entrance	0 to 30 g/s ± 0.15% of rate
Steam pressure	Baumer PMBH-24H23	Test section steam inlet	0 to 1379 kPa ±0.25% of span
Steam temperature	Type-T thermocouple	Test section steam inlet	-250 to 350°C ± 1.0°C
Sound level	REED 8080	1 meter from steam injection nozzle	30 to 130 dB ± 1.4 dB

2.2 Test Section

Our test section is identical to that of Thorpe et al.⁸ except that the back plate has been replaced with a quartz viewing window to enable image backlighting, significantly enhancing high speed visualization. The test section is shown in Fig. 2, where the process fluid flows from right to left and the steam is injected through an interchangeable nozzle at the bottom of the flow channel. The process fluid enters the test section through a flow straightener, after which the channel transitions from a standard 38.1 mm (1.5 in) diameter pipe to a rectangular cross section with a 26.24 mm height and 15.14 mm width. The rectangular section is 272.9 mm long, with the steam nozzle 152.1 mm downstream from the water entrance. Steam enters the test section via a nozzle machined into a brass plug, shown in the Figure 2 inset. Two quartz glass windows (38.48 mm wide and 26.24 mm tall) sit on either side of the nozzle, the rear for illumination by the high-power light and the front for video capture.

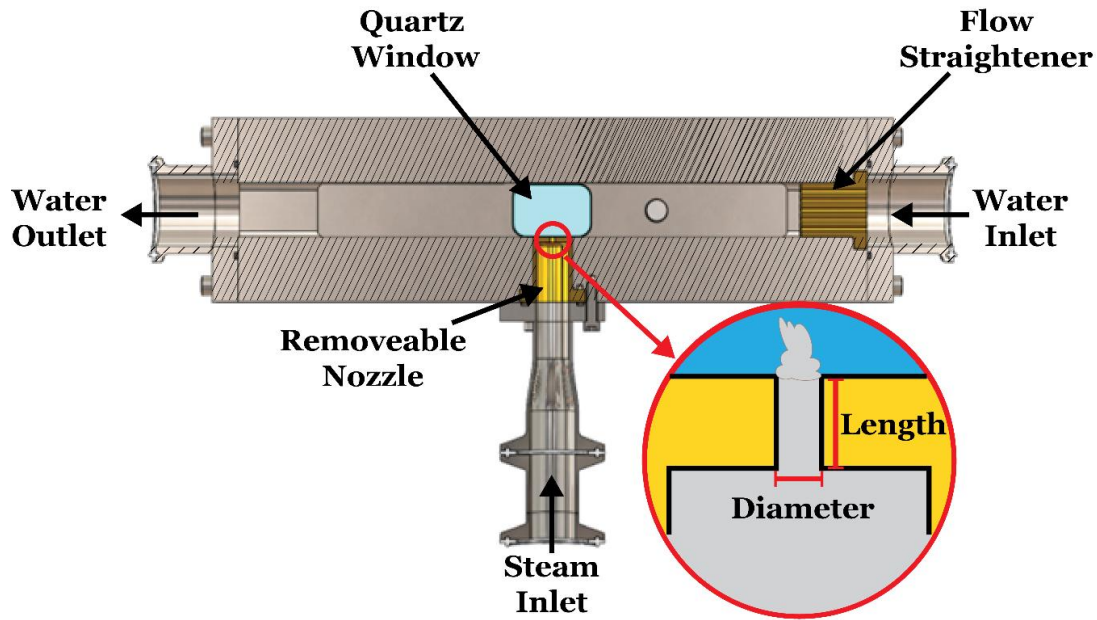


Figure 2: Schematic of test section and nozzle used in this study.

In a previous study, Thorpe et al. showed that small manufacturing defects can affect the behavior of nozzles dramatically.⁸ To avoid these defects, all the nozzles are fabricated with wire electric discharge manufacturing (wire EDM) so that they have a constant diameter throughout their length. Each nozzle is fabricated into a brass plug (Fig. 2) so that it can be easily replaceable between tests. The goal of this work is to investigate the effects of nozzle length and diameter on the stability of the steam plume and the associated noise. Three studies are performed (Table 2), two on single-port nozzles and one on a dual-port nozzle. In the first study, the diameter (D) of the nozzles is constant at 2.44 mm and the length varies between 1 and 8 times the diameter. In a second study, the length to diameter ratio (L/D) is held constant at 1, while the diameter varies between 1.65 mm and 3.18 mm. Finally, two dual-port nozzles with different diameters are evaluated in this work. These nozzles had a length-to-diameter ratio of 1 and are spaced 3.5 diameters apart to prevent the plumes from directly interacting with one another. This spacing still allows for adequate room to avoid any effects of wall interaction. The dual-port nozzles are

oriented perpendicular (both ports are at equal axial location with respect to the process fluid flow) to the flow.

Table 2: Nozzle geometry.

Study	Diameter (mm)	Length/Diameter (-)	Number of ports (-)	Spacing (diameters)
Vary L/D	2.44	1, 3, 6, and 8	1	-
Vary Diameter	1.65, 2.03, 2.44, 2.79, and 3.18	1	1	-
Dual Port	1.65 and 2.03	1	2	3.5

2.3 Flow Regime Characterization

Four primary flow regimes are observed in this study and follow the same nomenclature to Thorpe et al.⁸ These regimes are stable, condensation oscillation, transition, and unstable and are visually characterized in Figure 3. Each data point is manually classified into one of these four categories. All stable plumes have a single column of steam with no major bubble separation from the nozzle exit to plume tip. Additionally, the width of the plume is relatively constant with time. This flow regime is common at low process fluid temperatures. As the process fluid temperature increases, the flow transitions into the condensation oscillation regime. Condensation oscillation has a continuous plume (steam bubbles do not form), but the plume has more frequent radial perturbations and varying tip location over time. As shown in Figure 3, the condensation oscillation plume has a drastically different shape across the 0.75 ms shown. As the oscillations continue to increase in frequency, steam bubbles start to separate off from the main plume signaling a transition to the unstable regime. Other literature has referred to this transition regime as bubbling.¹⁸ After fully transitioning into the unstable regime, oscillations at the vapor-liquid interface increase in amplitude and the steam jet grows both radially and axially further into the process fluid. As shown

in Figure 3, bubbles eventually separate from the base of the unstable steam plume (attached to the nozzle exit) and oscillate as they continue to condense. The last regime in this study is the transition regime that occurs between condensation oscillation and unstable. This regime flips between periods of condensation oscillation and periods of unstable flow. The transitional steam plume emits a chirping noise as it oscillates in this regime. This flipping between regimes can be seen in the noise level plots such as Figures 4-5, where the span of decibel level is significantly larger than the other regions.

The high-speed videos are the primary data used to classify the flow regime, but the noise data is also considered for classifying the transition regime. It is possible that during data collection the video will only capture the condensation oscillation state of transition given the sample time is 1 second. Therefore, if within the 10 s of noise data collection the chirping noise characteristic of transitioning flow is heard, the plume will still be classified into the transition regime instead of condensation oscillation regime as indicated by the video alone. Similarly, it is possible for the video to only capture the unstable portion of transition, but within the noise level collection time frame if the chirping quiets to condensation oscillation levels. This too is classified as the transition regime.

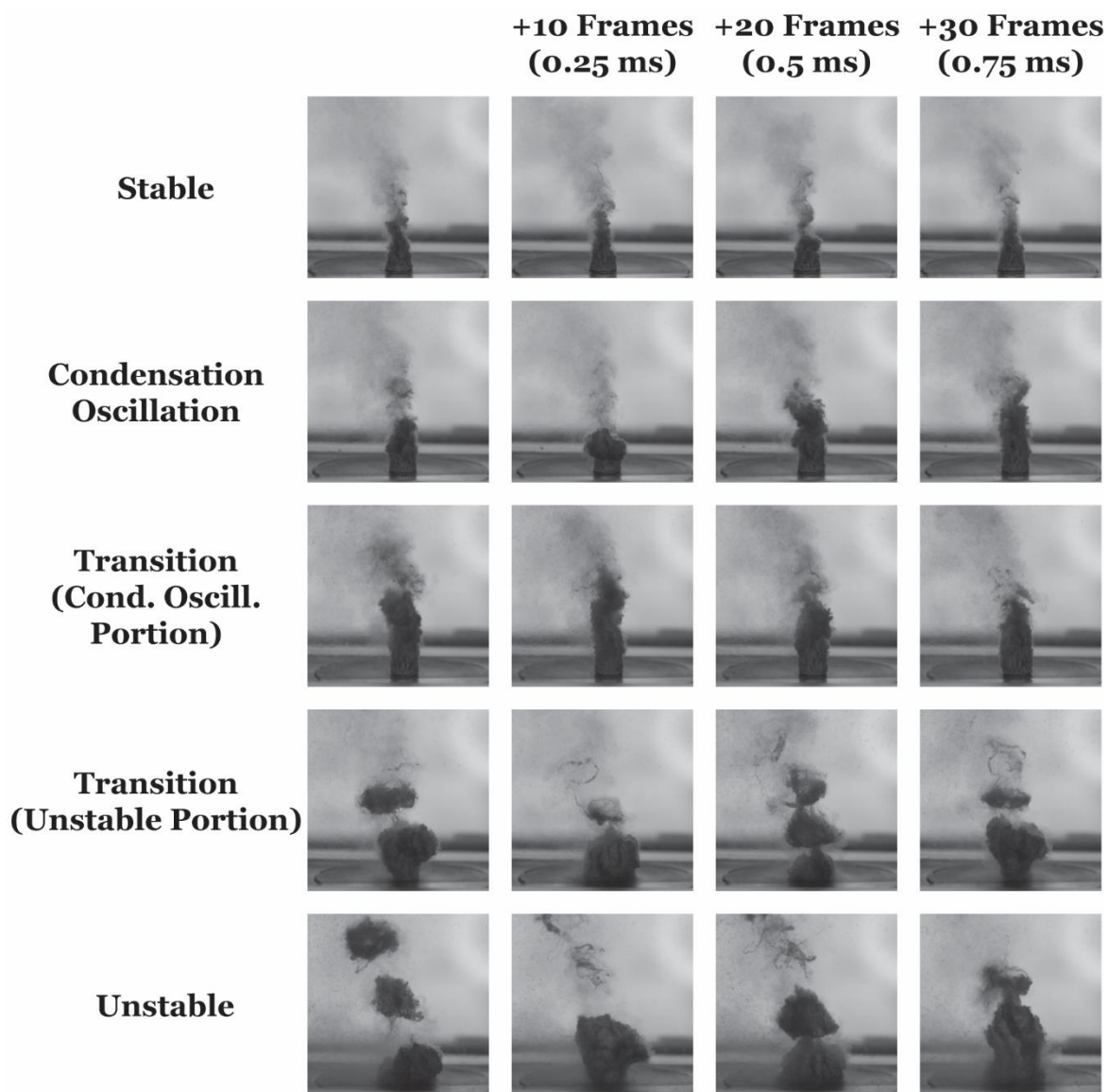


Figure 3: Flow Regime Sample Images. Videos of each flow regime can be found in the supplemental information.

Chapter 3: Results and Discussion

Three studies are performed to characterize the effect of nozzle geometry on flow regime and noise level. Only straight nozzles, meaning those with a constant cross-sectional area, are tested within this study; additional geometries have been evaluated by Thorpe et al.⁸ First, we show the effects of the nozzle aspect ratio (L/D) when the diameter is held constant. Next, we evaluate the impact of nozzle diameter while the aspect ratio is held constant. Finally, we distinguish between the effects of the nozzle diameter and the steam mass flow rate by measuring the noise generated by two nozzles side by side.

3.1 Effect of Length to Diameter (L/D) Ratio

Figure 4a and 4c show flow regimes for nozzles of varying lengths over a range of process fluid inlet temperatures when the water to steam pressure ratio is 0.47 and 0.58, respectively. These figures show that the process fluid temperature has a significant impact on the steam plume flow regime. At low temperatures for a given L/D , the flow regime is stable. Increasing the temperature reduces the condensation driving potential (difference between steam and process fluid temperatures) and results in an increasingly unstable plume. These results align with prior work that shows decreasing the condensation driving potential in DCC amplifies plume surface instabilities.^{4-6,14}

Although this general trend is seen for every nozzle, Figure 4a shows that the flow regime transition points shift to lower water temperatures when the nozzle length increases. For example, a nozzle with L/D of 1 reaches the fully unstable regime when the process fluid temperature is 75°C, whereas a nozzle with L/D of 8 is fully unstable at 65°C. Similar trends are also seen at higher pressure ratios (Figure 4c) – shorter nozzles delay transitions to more unstable flow regimes until higher process fluid temperatures.

As expected from literature, the changing flow regimes result in differences in the overall noise levels. As shown in Figures 4b, stable flow regimes at low process fluid temperatures produce low noise levels ($\lesssim 72$ dBa). As the flow transitions to condensation oscillation and transition, the noise level progressively increases. In the stable and condensation oscillation regimes, the noise is relatively consistent, as shown by the error bars (max and min of samples measured). However, in the transition regime, the noise level varies significantly over the 10 seconds that sound data is collected. This variation is due to the flow regime flipping between the quieter condensation oscillation regime and the louder unstable regime. Finally, at the highest process fluid temperatures, the flow is unstable and results in high noise levels (~ 90 dBa). This aligns with prior work that has shown that the unstable regime results in the highest pressure fluctuations² in DCC.

Since shorter nozzles produce more stable flows, they also tend to have lower noise levels at a given process fluid temperature and pressure ratio. For example, in Figures 4a and 4b at 60°C , the nozzles in the transition regime (L/D of 6 and 8) produce 87 dBa, whereas the two shorter nozzles, which are not yet transitioning, are quieter (80 dBa). However, once each nozzle is unstable, there is no effect of the length-to-diameter ratio on decibel level – all nozzles produce about 90 dBa. This plateau might be due to the frequency of bubble collapse. From the high-speed videos, each separating bubble appears to be collapsing at about the same frequency regardless of nozzle type. Additionally, the length of the nozzle does not have a large impact on the size of the collapsing bubbles, which may result in similar amplitude sound waves at the dominant frequency. In this study, sound frequency data is not analyzed, but in future work it could be used to better explain this sound plateauing phenomenon in the unstable flow regime.

Comparing the two pressure ratios shows that higher pressure ratios make the steam plume unstable sooner, and because the plumes are unstable sooner, they are louder at each corresponding temperature. Even though there is generally a higher noise level observed at higher pressure ratios due to the shifted regime transitions, once the flow is unstable the noise level again plateaus around 90 dBa at both pressure ratios.

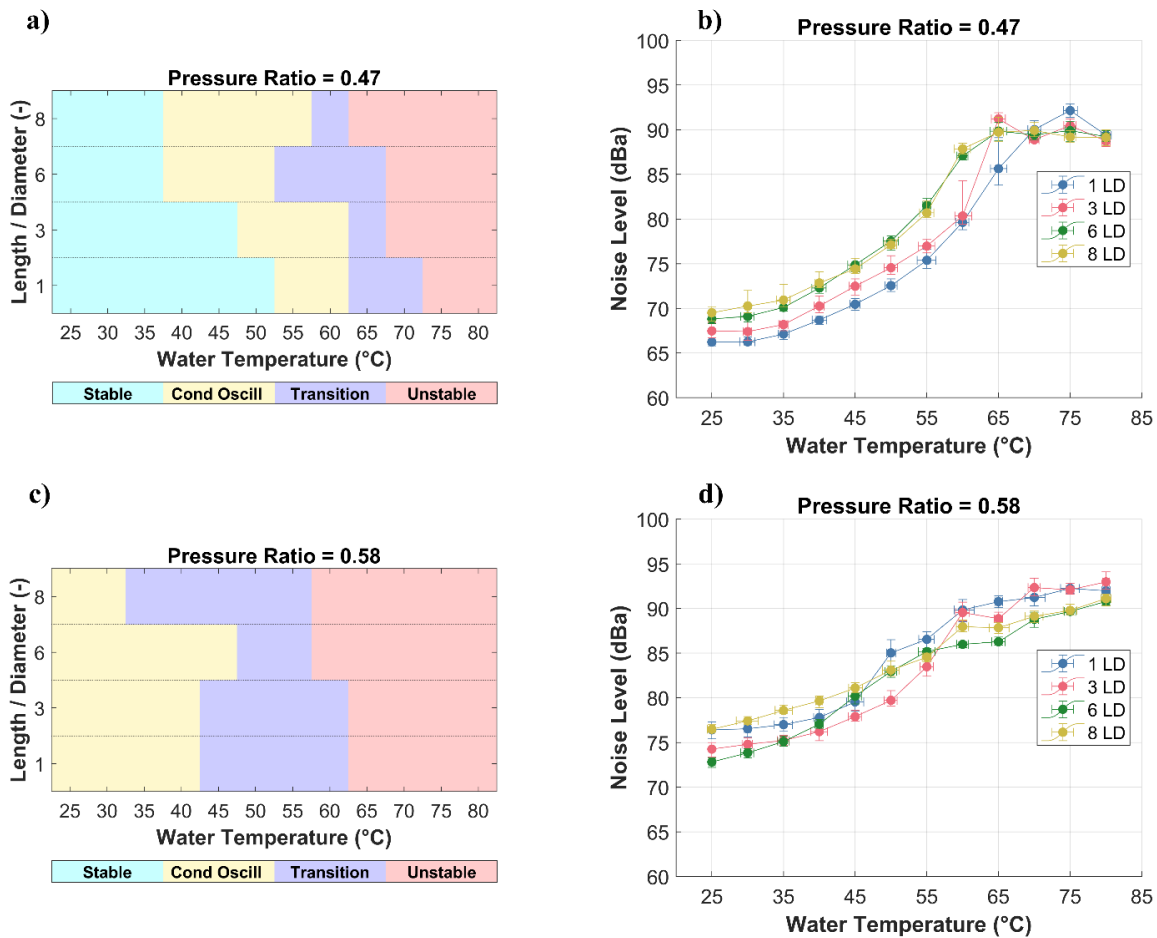


Figure 4: The (a) steam plume flow regimes and (b) noise levels over a range of process water temperatures and nozzle length-to-diameter ratios for a pressure ratio of 0.47. Similar plots for the (c) flow regimes and (d) noise levels are also shown for a pressure ratio of 0.58.

3.2 Effect of Diameter

A second set of five nozzles are evaluated with a length-to-diameter ratio of 1 and diameters between 1.65 to 3.18 mm. Figures 5a and 5c demonstrate the same progression of flow regime

with process fluid temperature. As the process fluid temperature increases (and the condensation potential decreases), the plume goes from stable, to condensation oscillation, then begins having short bursts of unstable plumes in the transition region, before becoming fully unstable with regular bubble formation. When the pressure ratio is 0.47 (Figure 5a), reducing the nozzle diameter delays transitions to more unstable flow regimes. Lowering the diameter has the largest impact on the stable flow regime, delaying the transition from stable to condensation oscillation by 20°C between the largest and smallest diameters tested. Smaller nozzles still delay the onset of subsequent regimes, but the impact is less marked. At a pressure ratio of 0.58 (Figure 5c), the results are similar but are somewhat less consistent. Overall, the 0.58 pressure ratio promotes more instabilities across a broader range of process fluid temperatures and the smaller nozzles delay transitions to more unstable regimes as the process fluid temperature increases.

As expected, these changes in flow regimes affect the noise level. Figure 5b shows the measured noise levels as a function of process fluid temperature at a pressure ratio of 0.47. The smallest nozzle ($D = 1.65$ mm) remains in the stable flow regime until the process fluid temperature is 60°C and produces a correspondingly low noise level ($\lesssim 70$ dBa). As previously observed, when the flow transitions into more unstable regimes, the noise level increases until it plateaus at a maximum value around 90 dBa in the fully unstable flow regime. The larger nozzles behave similarly but with much earlier transitions to unstable regimes. For example, the 3.18-mm diameter nozzle enters the condensation oscillation flow regime at a process fluid temperature of 40°C, which is accompanied by a sharp rise in noise level. In Figure 5d, all nozzles are fairly consistent in flow regime, and thus are consistent in their measured noise level.

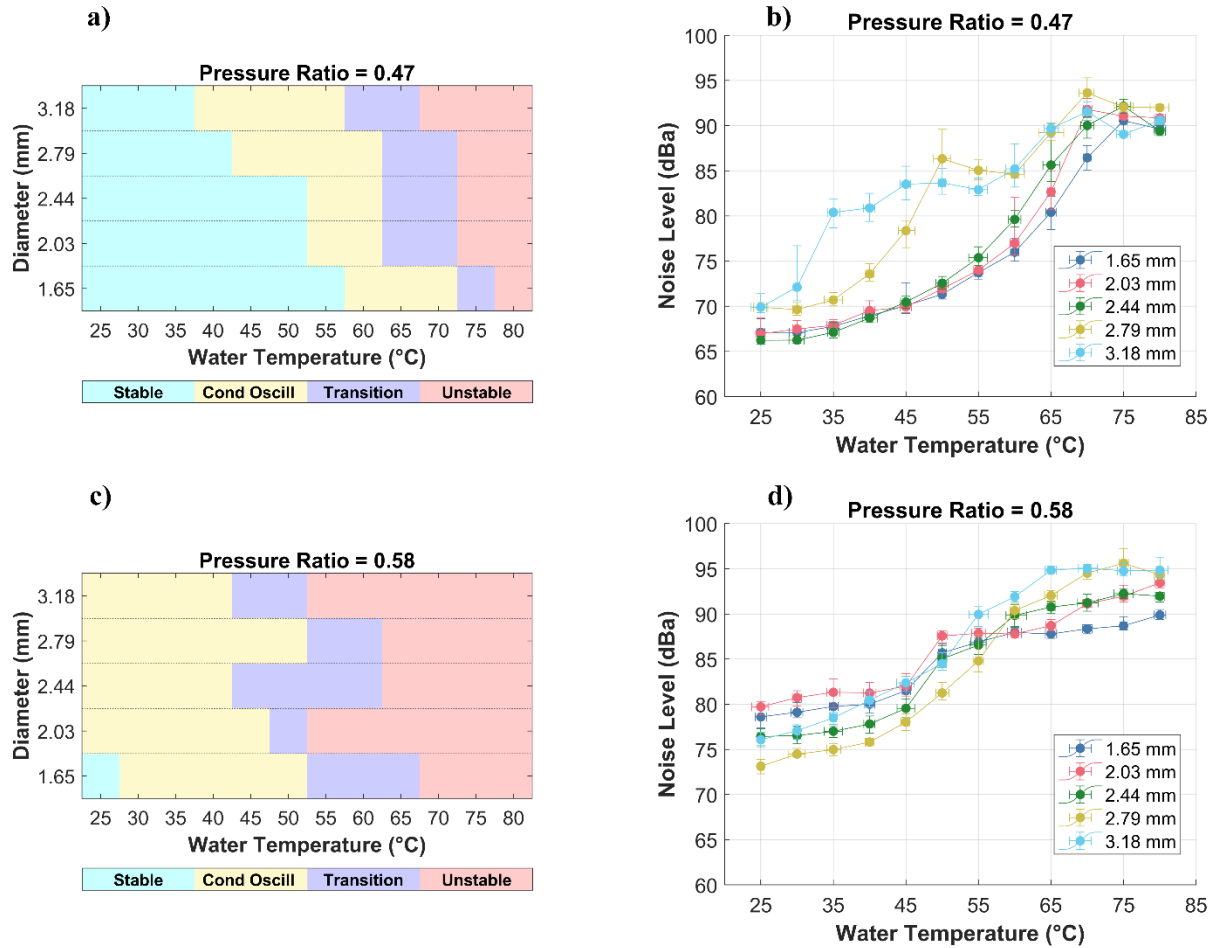


Figure 5: The (a) steam plume flow regimes and (b) noise levels over a range of process water temperatures and nozzle diameters for a pressure ratio of 0.47. Similar plots for the (c) flow regimes and (d) noise levels are also shown for a pressure ratio of 0.58.

3.3 Effect of Mass Flow Rate on Noise Level

Although the nozzle diameter has a significant impact on the DCC noise level, it also changes the steam mass flow rate (Figure 6). Comparing Figure 6 to Figure 5b, smaller diameter nozzles tend to be quieter and more stable, but also add less heat to the process fluid due to the lower steam mass flow rate. A final set of nozzles are evaluated to determine how diameter impacts noise for the same heat input. Specifically, two dual-port nozzles are manufactured with small ports that produce approximately the same total steam mass flow rate as one of the larger single-port nozzles discussed in section 3.2. The total mass flow rate of the single- and dual-port nozzles

are compared in Figure 6 based on the total cross-sectional area of all nozzles in the test section. Each two-port nozzle is designed to have two direct comparisons, one of the same nozzle geometry and one of the same steam mass flow rate. The average mass flow rates reported in Figure 6 are at a pressure ratio of 0.47. However, these mass flow rates are approximately the same when the pressure ratio is 0.58 because both correspond to choked flow and only the outlet pressure is adjusted, so the inlet steam density is constant.

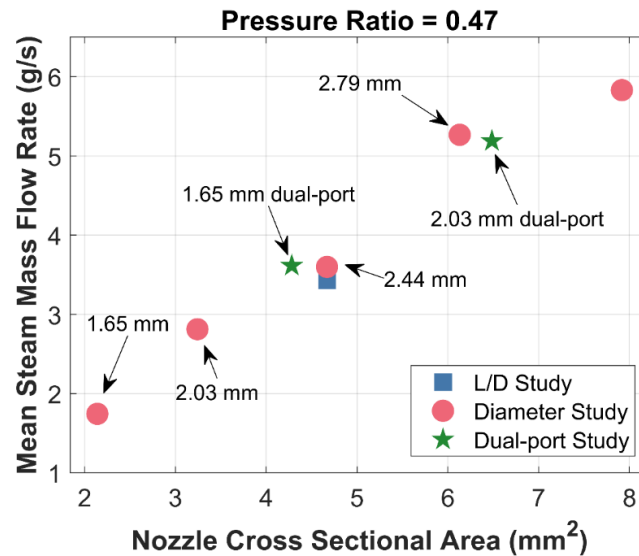


Figure 6: Mean steam mass flow rate of all single-port and dual-port nozzles evaluated in this paper at a pressure ratio of 0.47. The steam mass flow rates are nearly identical for a pressure ratio of 0.58 (within the uncertainty of the mass flow meter) because the steam flow is choked.

The dual-port nozzles are evaluated in the perpendicular orientation, meaning that the two nozzles are side by side at the same axial location in the process fluid channel. This orientation is chosen so that both plumes see the same process fluid temperature. Using a parallel orientation (where the second nozzle is directly downstream of the first) would force the downstream nozzle to condense in a higher temperature fluid pocket, thus changing its condensation dynamics.

The overall noise levels produced by the dual-port nozzles are shown in Figure 7. For most conditions, two smaller nozzles are quieter than one larger nozzle that produces the same steam

flow rate. This indicates that mass flow rate is not a dominant factor in the noise level. Additionally, the two-port nozzle produces either the same or lower noise levels than a single-port with the same diameter (but lower flow rate) except for the 1.65-mm diameter dual-port nozzle operating at a 0.47 pressure ratio (Figure 7a). For this case, when the process fluid temperature is low, the dual-port nozzle produces higher noise levels than a single-port nozzle of the same geometry. The increased noise levels for these conditions are the result of flow regime differences between the two nozzles. The flow regimes of the dual-port nozzles are not systematically classified because the two plumes overlap in the videos and are difficult to visually separate. However, it can be observed from the high-speed video data that both plumes appear to be in condensation oscillation for most temperatures and pressure ratios. The dual-port nozzles unexpectedly stay in the condensation oscillation regime far longer than the single-port nozzles. For the conditions in Figure 7a, the dual-port nozzle does not appear to reach the transition flow regime until 75 or 80°C, whereas the single-port nozzle with the same geometry reaches this regime at 75°C as shown in Figure 5a. Additionally, although the two nozzle plumes do not seem to overlap, the width oscillations in the condensation oscillation flow regime are out of phase with each other, meaning that the second plume influences the flow features of the first. While not part of the analysis of this study, more work is needed to understand flow regimes and plume interactions in multi-port DCC nozzles since it seems to have a significant impact on the overall noise level. Ultimately, none of the dual-port nozzles reach the 90 dBa plateau characteristic of unstable flow (as described in sections 3.1 and 3.2), because the steam plumes never reach that regime.

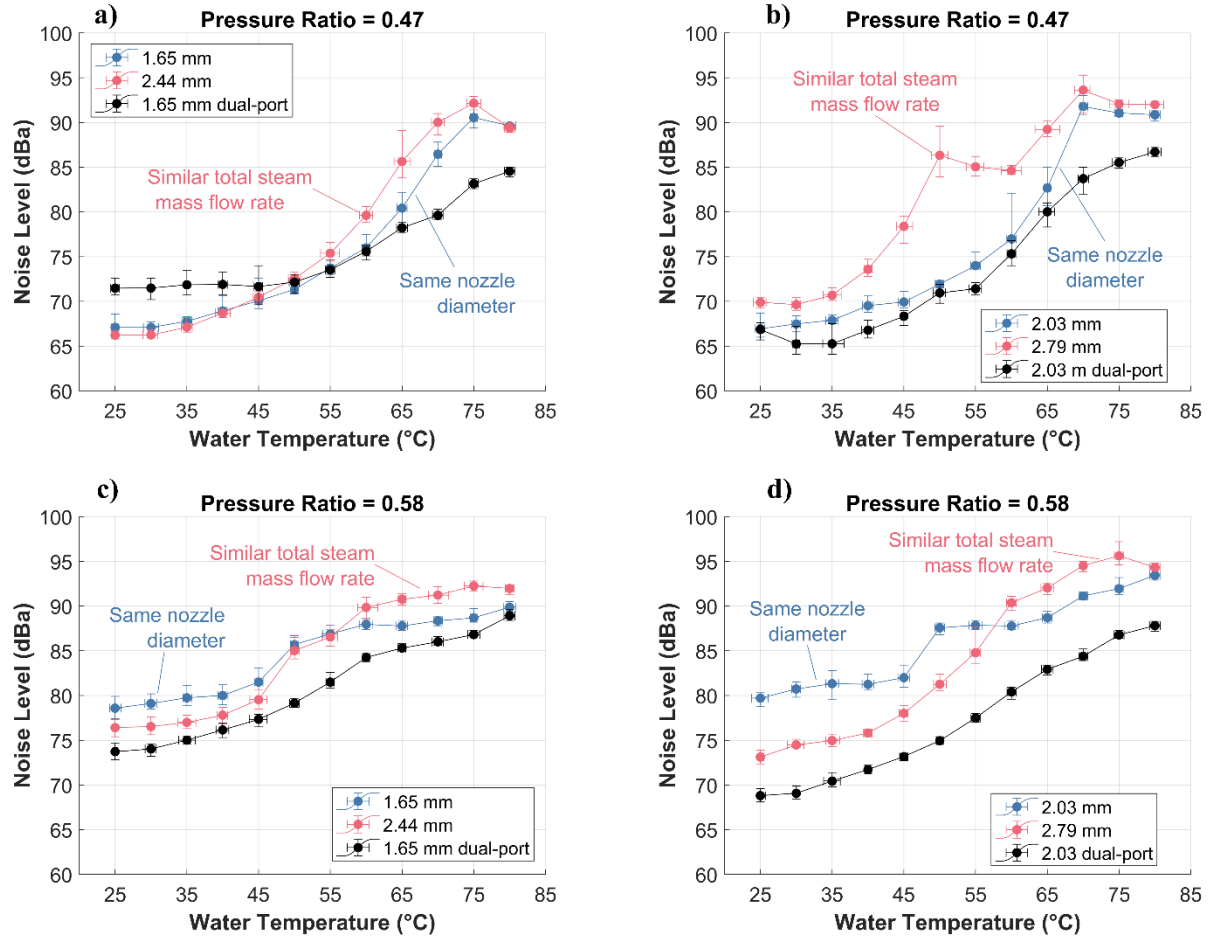


Figure 7 : The noise levels for the 1.65 mm two-port nozzle with its geometric single-port and mass flow single-port peers at a pressure ratio of (a) 0.47 and (c) 0.58 over a range of process water temperatures. Similar noise level plots for the 2.03 multiport study at a pressure ratio of (b) 0.47 and (d) 0.58.

Chapter 4: Conclusion

This work presents the results of both measured noise level based on OSHA 1910.95 App G and plume flow regime. A parametric investigation is conducted on nozzle length, diameter, and number of ports in order to better understand what impact each has on plume stability and noise level. The key results from each study are reported below:

1. A smaller length-to-diameter ratio promotes stability at higher process fluid temperatures and results in an average noise reduction of 5 dBa, where the total noise levels measured are between 70 and 90 dBa.
2. Nozzles with larger diameters tend to significantly increase the overall noise level until the unstable flow regime is reached; in the unstable regime, all nozzles produce roughly the same noise (~90dBa).
3. Multiple smaller nozzles can achieve the same mass flow rate as a single larger nozzle with less noise at most process water temperatures. However, if the larger nozzle operates within its stable regime, the use of multiple nozzles may increase noise levels.
4. Mass flow rate does not drive changes in the overall noise level, flow regime does.

Although this work provides some initial data on how multiple nozzles behave in crossflow DCC, more work is needed to understand the impacts of nozzle spacing and orientation on these conclusions. Future dual-port nozzle studies should further investigate flow regimes, focusing on how plume interactions impact the flow regime. Additionally, more work is needed to correlate some of the plume flow features to the noise level. Utilizing image processing to quantify the area changes of the plumes would be beneficial but is a difficult task when the plumes are in line with the camera perspective. Finally, more work is needed to understand how orientation in the process fluid stream impacts the performance of multi-port nozzles.

References

1. Hong, A. *et al.* Experimental study of interface behavior and sound pressure oscillation of direct contact condensation of a steam jet in flowing water. *Experimental Thermal and Fluid Science* **150**, 111054 (2024).
2. Alden, Z. R., Maples, G. D., Dressler, K. M., Nellis, G. F. & Berson, A. Plume Stability During Direct Contact Condensation of Steam in a Crossflow of Subcooled Water, at High Mass Flux and With a Small Nozzle Diameter. *Journal of Heat Transfer* **143**, 091602 (2021).
3. Zhao, Q. & Hibiki, T. Review: Condensation regime maps of steam submerged jet condensation. *Progress in Nuclear Energy* **107**, 31–47 (2018).
4. Kerney, P. J., Faeth, G. M. & Olson, D. R. Penetration characteristics of a submerged steam jet. *AIChE Journal* **18**, 548–553 (1972).
5. Sanaullah, K. *et al.* Determining potential of subcooling to attenuate hydrodynamic instabilities for steam–water two phase flow. *International Journal of Heat and Mass Transfer* **84**, 178–197 (2015).
6. Khan, A., Haq, N. U., Chughtai, I. R., Shah, A. & Sanaullah, K. Experimental investigations of the interface between steam and water two phase flows. *International Journal of Heat and Mass Transfer* **73**, 521–532 (2014).
7. Pellegrini, M., Naitoh, M., Josey, C. & Baglietto, E. Modeling of Rayleigh-Taylor Instability for Steam Direct Contact Condensation. (2015).
8. Thorpe, C., Berson, A. & Mahvi, A. Shock location effect on direct contact condensation stability. *International Journal of Heat and Mass Transfer* **214**, (2023).
9. Chen, X. *et al.* Visualization study on direct contact condensation characteristics of sonic steam jet in subcooled water flow in a restricted channel. *International Journal of Heat and Mass Transfer* **145**, 118761 (2019).
10. Xu, Q., Guo, L. & Chang, L. Mechanisms of pressure oscillation in steam jet condensation in water flow in a vertical pipe. *International Journal of Heat and Mass Transfer* **110**, 643–656 (2017).
11. Xu, Q. & Guo, L. Direct contact condensation of steam jet in crossflow of water in a vertical pipe. Experimental investigation on condensation regime diagram and jet penetration length. *International Journal of Heat and Mass Transfer* **94**, 528–538 (2016).
12. Cho, S., Song, C.-H., Park, C.-K., Yang, S.-K. & Chung, M.-K. Characteristics of pressure oscillation induced by direct contact condensation of steam discharged through sparger in a pool of subcooled water.
13. Simpson, M. E. & Chan, C. K. Hydrodynamics of a Subsonic Vapor Jet in Subcooled Liquid. *Journal of Heat Transfer* **104**, 271–278 (1982).
14. Kim, H. Y., Bae, Y. Y., Song, C. H., Park, J. K. & Choi, S. M. Experimental study on stable steam condensation in a quenching tank. *International Journal of Energy Research* **25**, 239–252 (2001).
15. Chong, D. *et al.* Research on the steam jet length with different nozzle structures. *Experimental Thermal and Fluid Science* **64**, 134–141 (2015).

16. Quddus, A. *et al.* Experimental study on steam plume shape characteristics for bevelled spray nozzles exhausting into quiescent water. *Nuclear Engineering and Design* **394**, 111824 (2022).
17. Chong, D., Yue, X., Wang, L., Zhao, Q. & Yan, J. Experimental investigation on the condensation patterns and pressure oscillation characteristics of steam submerged jet through a horizontal pipe at low steam mass flux. *International Journal of Heat and Mass Transfer* **139**, 648–659 (2019).
18. Chan, C. K. & Lee, C. K. B. A regime map for direct contact condensation. *International Journal of Multiphase Flow* **8**, 11–20 (1982).

Appendix A: Loop Startup/Operation Instructions

A.1 Safety

1. If you are not completely comfortable running the loop, operate with someone who is fully trained. If you have questions, ASK!
2. Wear safety glasses when operating the loop.
3. Wear steam-proof gloves when operating the steam line or anything hot.
4. Look away when opening valves or circuit breakers so as to protect the face if there is a leak.
5. Clean up any water spills on the floor with a mop in the room immediately to prevent dripping into the room below.
6. Make sure you understand where the drains go and where the emergency drains are before turning on the steam generator.
7. If anything is unsafe, do NOT continue testing. We can always try another day.

A.2 Emergency shutdown

1. Immediately shut the steam injection valve if it is open.
2. If it is something drastic (a large leak, something blew), skip directly to the Loop Shut Down procedure (see section A.9) and turn the loop off as quickly as possible.
3. Turn off the steam generator first if it is a steam problem. Turn off the pump first if it is a water problem.

4. If it is something that prevents further data collection but does not pose a safety risk if the loop is shut down, proceed to the Collecting Reference Picture procedure (see section A.8). This does not require the steam to be on, so that may be shut down first.
5. Isolate where the problem is and reach out to the superuser for resolution (if you think you can fix it on your own, at minimum alert the superuser so they are aware of what is going on). If you are the superuser and have questions, please set up a working meeting with Dr. Mahvi and we will resolve the issue together.

A.3 Start-up

1. Check loop for any leaks, noticeable things wrong, etc.
2. Plug in both 120 V extension cords into outlet near the ground by the annular flow experiment (the two white sheathed cords in Figure A1).

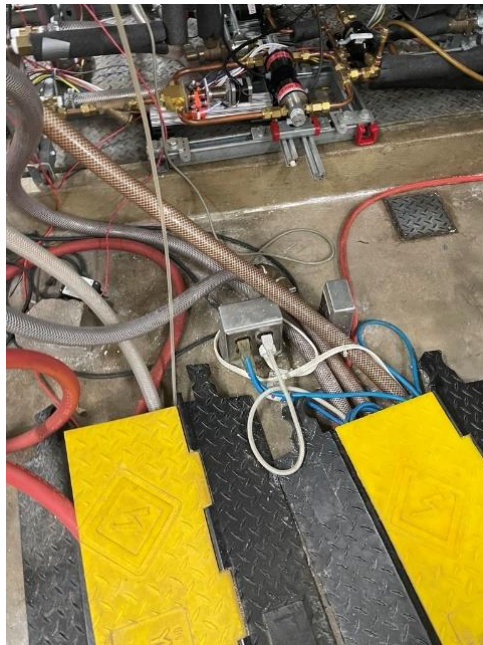


Figure A1: Extension cord location for DAQ power.

3. Turn on the scale for the bladder tank (Figure A2).



Figure A2: Photograph of the bladder tank scale readout.

4. Open the water loop bottom drain valve, water loop top drain valve, top air valve, city water heat exchanger drain valve, front steam drain valve, steam line drain valve with condensate trap, and back steam line drain valve. These values are shown in Figure A3. Note: The three valves associated with the deaerator tank and steam generator **MUST** be closed unless testing to prevent water from siphoning out of the deaerator tank.

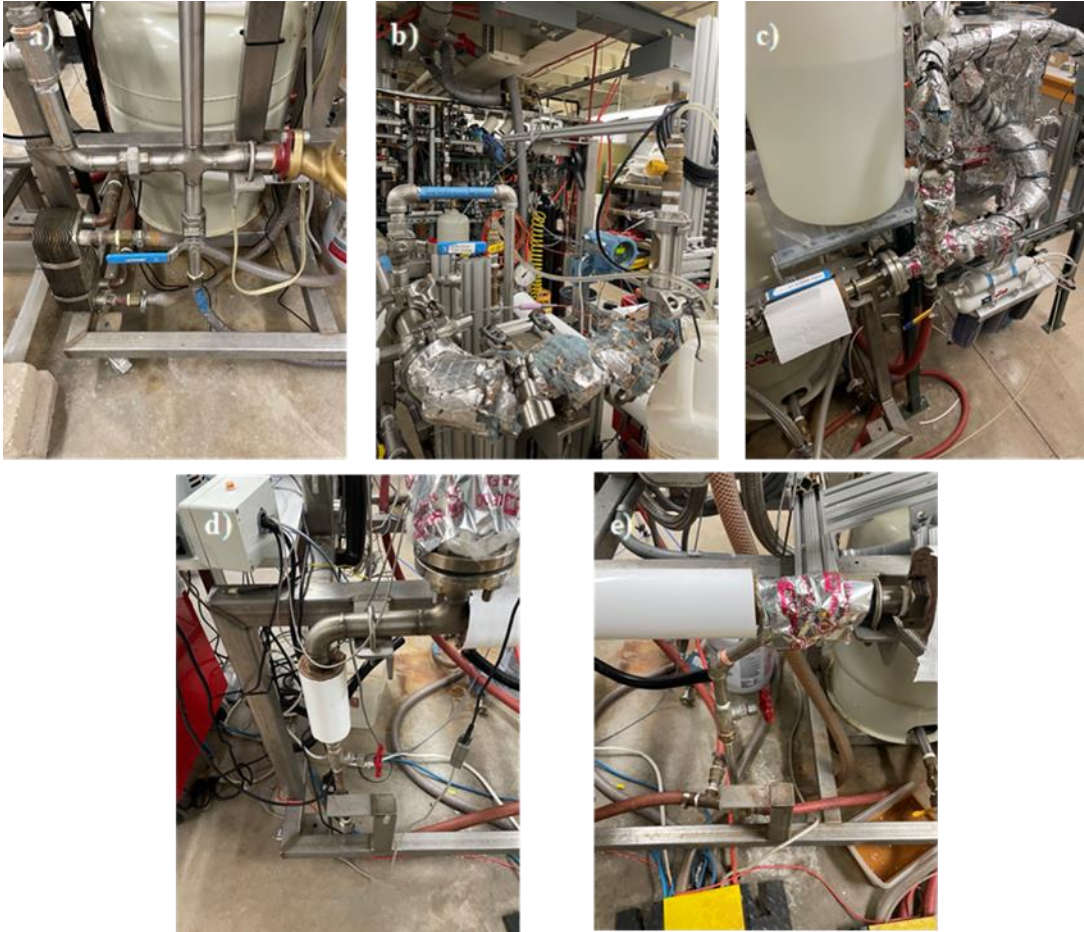


Figure A3: a) Water loop bottom drain valve, b) water loop top drain valve and two top bleed ports, c) steam cross, d) steam line drain valve with condensate trap, and e) back steam drain valve.

5. Open or download the “Master Steam Injection LabView” folder in the “Test Rig Master” folder from Box or the MFVAL share drive under ‘Steam Injection’ If you do not have access, contact a graduate student in the MFVAL for instructions.
6. While all files are needed to run the program, only open ‘The_boss’ as this is the top-level interface. All other subprograms are called by the Boss.

Name	Date modified	Type	Size
Audio	8/27/2019 4:32 PM	LabVIEW Instrume...	86 KB
Data_Analysis_Open	7/10/2019 3:15 PM	LabVIEW Instrume...	14 KB
Dynamic_Collection	3/6/2020 4:42 PM	LabVIEW Instrume...	19 KB
Format_Data	8/2/2019 2:17 PM	LabVIEW Instrume...	21 KB
Master_Steam.aliases	3/12/2020 11:15 AM	ALIASES File	1 KB
Master_Steam.lvpls	9/15/2019 11:04 PM	LVLPS File	1 KB
Master_Steam	9/15/2019 11:04 PM	LabVIEW Project	35 KB
PressureCal	8/6/2019 8:48 AM	LabVIEW Instrume...	206 KB
Process_Collection	7/10/2019 4:26 PM	LabVIEW Instrume...	14 KB
PtoTSat	6/26/2020 3:52 PM	LabVIEW Instrume...	165 KB
SatPSatT	7/10/2019 3:46 PM	LabVIEW Instrume...	11 KB
Save_Path_Creation	8/27/2019 3:47 PM	LabVIEW Instrume...	75 KB
The boss	7/2/2020 9:41 AM	LabVIEW Instrume...	3,480 KB

Figure A4: “The_boss” LabView file location.

- The front panel will probably look like that of Figure A5, otherwise you may be on another tab, click the white arrow on the ribbon to run the program.

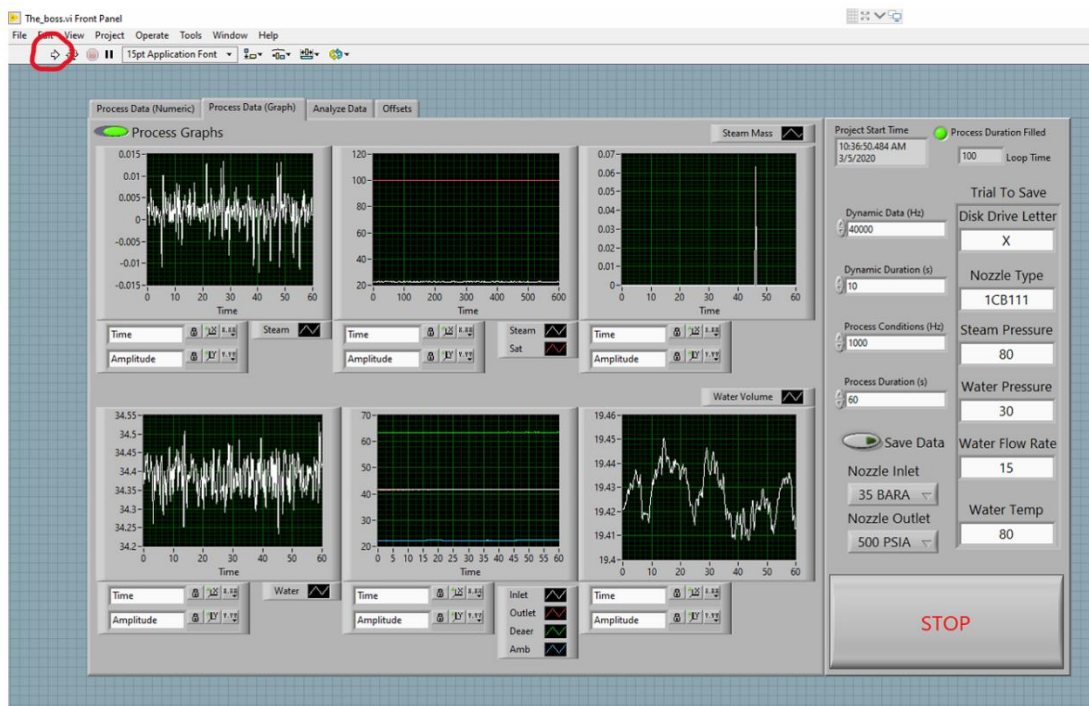


Figure A5: Front panel of “The_boss” LabView program for data collection.

8. Launch R8080 software and set up the second monitor as shown in Figure A6.

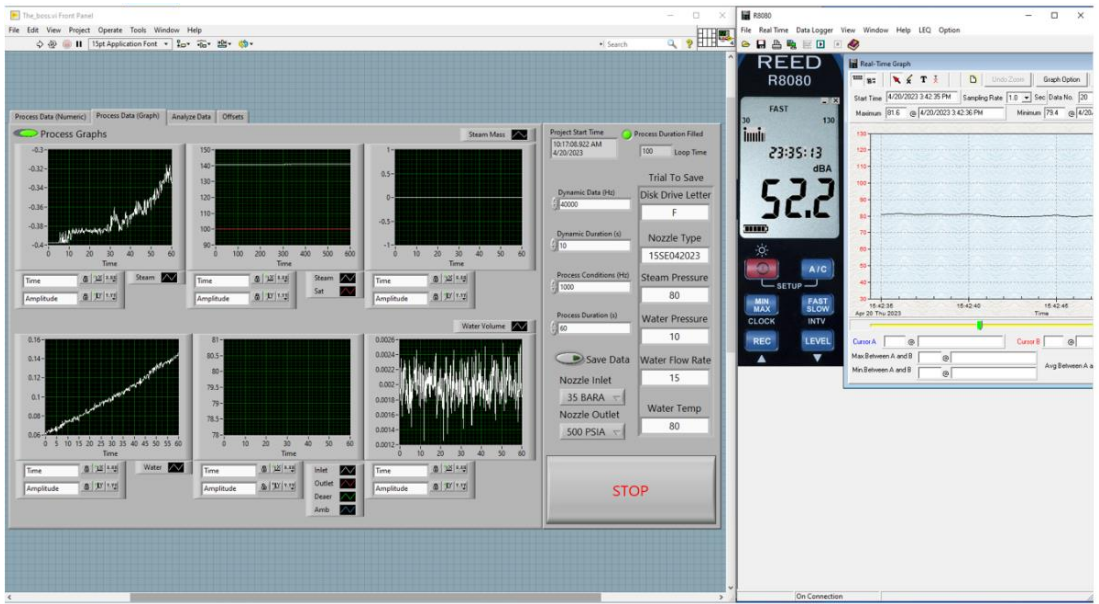


Figure A6: R8080 software next to LabView front end.

9. Click the 'offsets' tab and click 'remove offsets'.

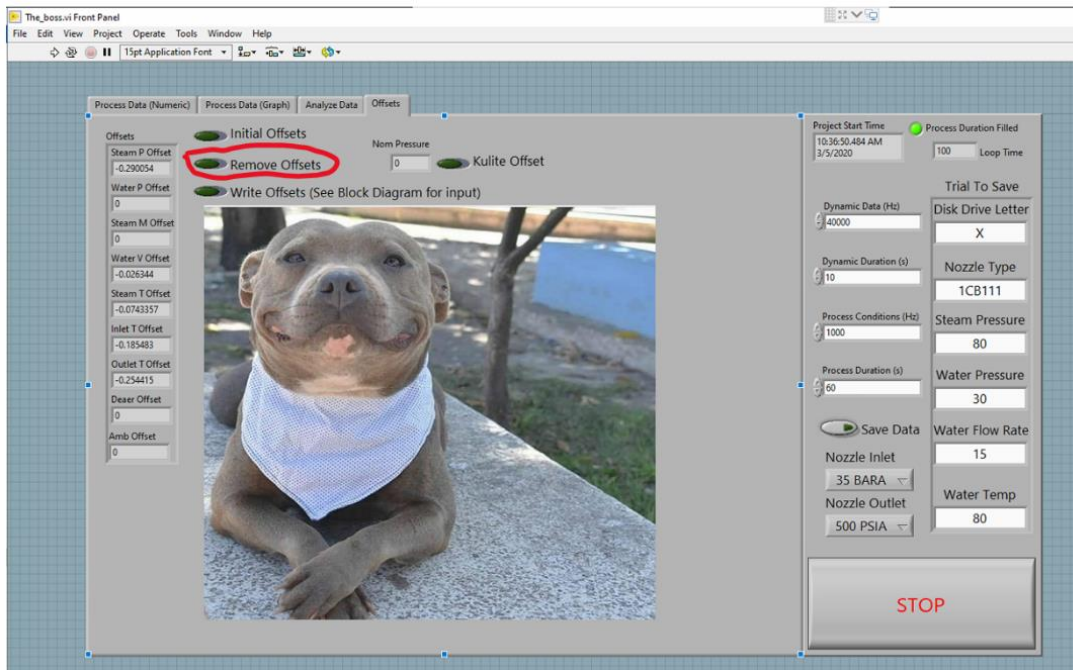


Figure A7: "The_boss" offset tab.

10. Click the ‘process data (graph)’ tab and check that all data looks to be ‘normal’.

- By normal, I mean that the pressure graphs are roughly around zero or some offset less than 1, the steam mass flow is zero, the water volume is roughly zero, and the temperatures are not changing with time and roughly within a degree from the ‘ambient’ thermocouple at the top of the sound level meter boom.
- If any of these are not normal (most likely the steam mass flow or temperatures), either vent out the system with the compressed air valve next to the computer station to get the mass flow down, open other valves, especially at the bladder tank entrance, to get rid of any stored water, or wait for the values to return to a reasonable value. If you vent the system with compressed air, you must wait for the thermocouples to come back to room temperature and a steady value (this will take a while).

12. Go back to the ‘process data (graph)’ tab and let a full minute of good data run again, the graphs should not show an offset by the end of it and be steady. Change the fields in the “Trail to Save” box on the right of Figure A7 to the values listed in a – f below and click the “Save Data” toggle switch. This will generate a saved file that can be read by MATLAB for processing.

- a) Set disk drive letter: Enter the correct drive. We are currently using the E drive (December 2024).
- b) Set nozzle type: for ambient, specify the file name using the following convention: ‘AMBTodaysDate’ (e.g., AMB072224)
- c) Set “steam pressure” = 0

- d) Set “water pressure” = 0
 - e) Set “water flow rate” = 0
 - f) Set “water temp” = 0
13. If using decibel meter, press the play button in the r8080 software and select 20 samples at a rate of 0.5 seconds.
- a) Do step 13 while the software is recording.
 - b) Save the data in the folder created by LabView and save the data as AMBTodaysDate-0-0-0-0-db.
14. After ensuring that the ambient data is properly collected (if you change anything in the loop after this, collecting ambient conditions will be much harder). Turn on the 480 V breaker on the ceiling leading to the steam generator (you may need a step stool, look around the lab).
15. Check the deaerator tank to ensure that it is filled, if not, fill it with filtered water.
16. Check that the storage tank leading to the deaerator tank is filled, if not, fill it with filtered water so that the pump will not be filled with air.
17. Ensure the Manual Controlled power supply to the deaerator fill pump and buffer tank is on (usually kept on). The pump between the buffer tank and DA tank operates off a **manually operated** switch to prevent cold water from mixing with the DA hot water. With the power supply on, the Reverse Osmosis filter will be able to constantly fill the buffer tank as it takes a long time to make clean water.

18. Turn on the two switches on the steam generator, check that the temperature set point is zero (change it NOW if otherwise), the red valve leading from the deaerator tank to the steam generator is open, and the yellow valve from the pump is directed to only the steam generator and not the water loop.
19. Change the temperature set point to 130°C, watch for pressure fluctuations on the pressure gauge, and vent out the water collected at the bottom of the steam line leading from the steam generator using the yellow valve. Close the yellow valve after 5 seconds to allow the steam to recollect.
20. Slowly open the red valve leading to the deaerator tank from the steam generator and let the tank heat up. It should automatically close around 85°C, but the red valve should be closed when the heating process is complete (80-85°C). The tank is heated to get air bubbles out of the water that may affect testing, so try to keep the tank heated above ambient. This step will take around 20 minutes.
21. Change the temperature set point on the steam generator to 0°C.

A.4 De-aerate the Loop

1. Close water loop bottom drain valve, ensure yellow valve connecting air separator and steam mass flow meter is open, and the valve after the steam mass flow meter is directing flow into the bladder tank.
2. Ensure the water loop top drain valve, all the valves in the water loop flow path, and top air valve are open.

3. Turn the water loop pressure up to 30 psi using the air dial located on the air line leading to the bladder tank.
4. Once the black steam generator pump has stopped, shut the valve leading from the pump to the steam generator.

Note: The next 4 steps happen quickly. Read ahead so you are ready.

5. While opening the valve leading to the test loop, turn on the override switch on the side of the steam generator to turn on the pump.
6. When water has filled to the top of the sight glass, close the top drain valve. When most air has left the glass sight on top of the loop, close the top air valve. **Caution: If the steam pump does not shut off after flipping the override switch, do not close the valve leading to the water loop.** Attempt to shut off the Temp Controller Switch and then the Disconnect Switch on the Steam Generator panel. To fix this issue, turn off the two steam generator power switches and the override switch on the side. Then change the steam generator pump valve pathing to run to the steam generator instead of the water loop. Only when the valving is directing flow to the steam generator, then turn the panel back on and flick the override switch on and off again and wait a couple seconds and it will stop when the float switch on top of the generator is satisfied.
7. When the scale for the bladder tank has raised by about 10 lbs, turn off the override switch on the side of the steam generator control panel and simultaneously close the valve leading to the water loop from the steam generator pump.
8. Turn on the gold water loop pump by first turning on the pump electrical control disconnect and then turn the “pump start” switch from off to on.

- a) If the pump does not turn on immediately, repeat step 8.
9. Wait 10 seconds, then close water loop pump recirc valve fully
10. Vent air you see in the sight glass on the top of the loop while the loop is deaerating.
11. Partially close the yellow valve in the water loop after the heat exchanger, but before the air separator to reduce the pressure to help alleviate bubbles. This valve will also be used to control the flow rate in the loop.
12. Occasionally close and open the top drain and back bleed valves to remove trapped air.
13. While the loop is deaerating, you can prepare the camera. See section A.5.
14. Deaeration is considered complete when there are no visible bubbles in the flow path or sight glass, this can take anywhere from 10 minutes to 2 hours.
 - a) If the loop is not fully or mostly deaerated within 1 hour (and has not improved at all) the process should be repeated.
 - b) Drain the water side of the loop (follow section A.9 for water drain) and then restart from the top of section A.4.

Note: Opening the steam injection valve may bring air back into the system. Open and close the valve to remove air from the steam line, and re-deaerate the loop, as necessary. The steam line may need to be re-prepped. See section A.6 for more details.

Troubleshooting: If you are struggling to remove air from the loop, try injecting steam into the loop until the water reaches 70°C. This may be helpful and there is no need to fully prep the steam

for this as you won't be taking data. If this does not work, try cutting off the steam and letting the loop cool to $\sim 20^{\circ}\text{C}$ and circulate at this temperature for 30 minutes.

A.5 Prep the Camera

1. When using the camera, coordinate with others in the lab to make sure there are not two experiments running simultaneously that need it.
2. The Phantom camera is most likely stored in the back side room in a Pelican camera case. Be careful carrying it, as it is very expensive.
3. The camera stand should be by the test section. A nut on the stand should screw into the bottom of the Phantom camera to secure it to the camera stand. You will need a flathead screwdriver.
4. A red, yellow, and black cord need to be attached to the back of the camera.
 1. Red: power cable leading to power outlet, attach to power port on camera
 2. Yellow: ethernet cord heading to ethernet attachment on front of desktop, attach to first ethernet port on camera
 3. Black: trigger cable leading to BNC cable leading to data acquisition box, attach large end to associated port on camera, other end may need a male-to-male adapter to connect the two female BNC ends
5. Attach lens from computer station to the front of the camera. Keep all lens caps nearby when you are done so they are easy to locate. If you can't find the lens, ask the superuser.
6. Open PCC software on the computer, click the dropdown under the 'live' tab and add the camera. The ID is 12101.

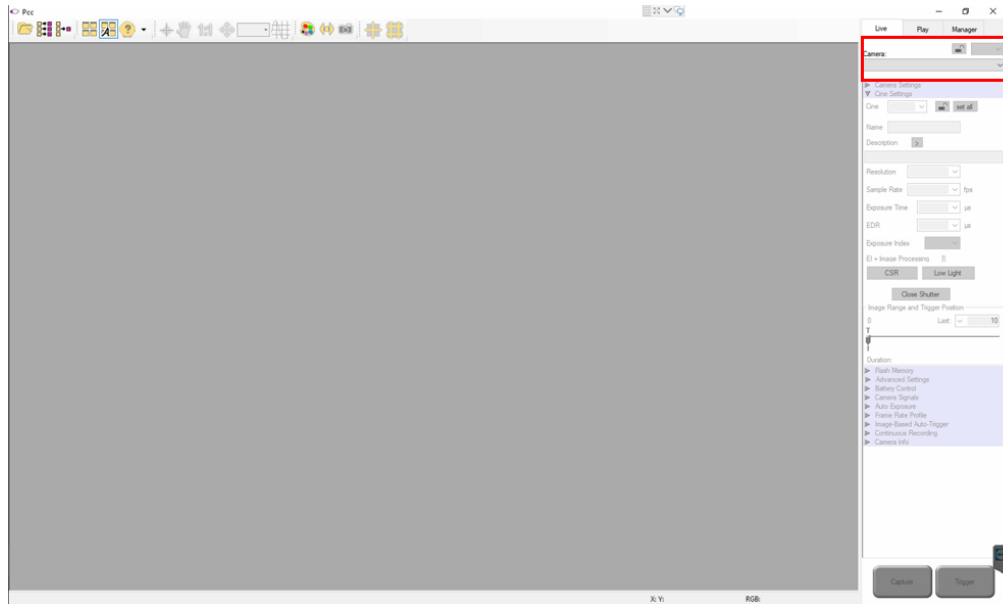


Figure A8: Phantom Camera Control software front panel upon opening.

7. If the image shown looks like static, go to the 'manager' tab, click the blue, red, and grey triangle at the bottom, and click 'Load Factory Stg...'. This should reset the camera.

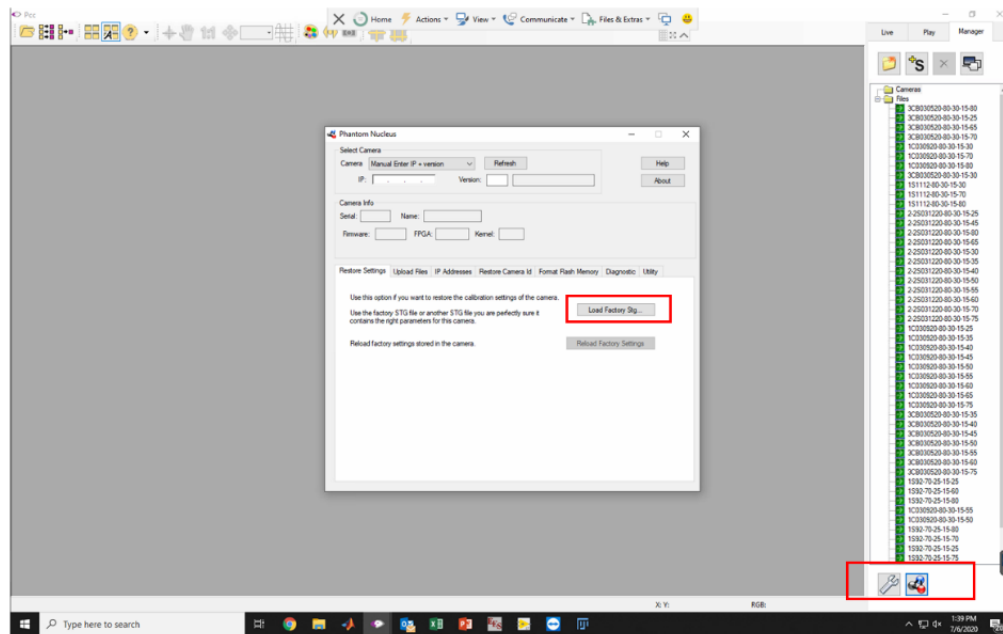


Figure A9: PCC video manager menu.

8. Before taking any video, click 'CSR' on the 'Live' tab to reset the field of view. You will have to do this every time you change the video resolution.

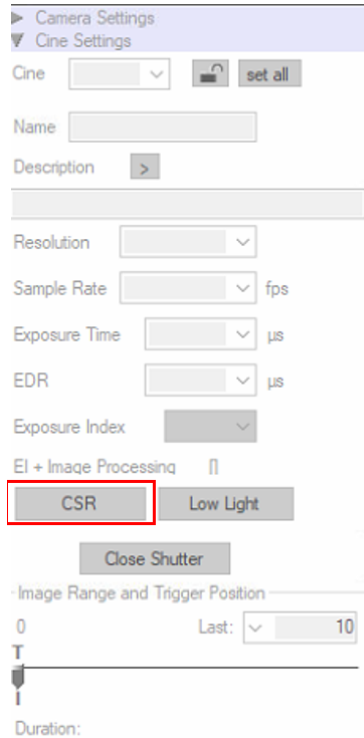


Figure A10: Cine and Camera settings from the front end of PCC.

9. When looking at video for deaeration, the resolution can be much higher than actual testing, about 512x512 should work for viewing the window. The sample rate can be anywhere from 100-20,000 and the exposure time can be adjusted to view the window as cleanly as possible.
10. Take the lens cap off and turn on the LED back light when you want to view the videos. Turn off the LED panel when it is not in use – it can overheat. The shutter can be opened or closed, the focus can be changed, and the aperture size can be changed through actions on the lens.
11. When collecting data, the camera should be focused on the steam plume and the light should be bright to allow for fast exposure times. The camera CANNOT be moved once you have started taking data. When you are ready to test, the camera settings should be:

- a) Resolution: 256x256
- b) Sample Rate: 40,000 fps
- c) Exposure time: lowest possible, 1.00
- d) EDR: 0
- e) Image Range and Trigger Position: the slider should be at the zero position.

A.6 Prep the Steam

1. Open the front steam drain valve (see Figure F6) and the drain valve on the steam trap (valve in Figure A3d).
2. Turn on the steam generator and set the set point temperature to 130°C.
3. Open and close the yellow valve at the base on the steam generator discharge again to get rid of any water buildup.
4. When the steam has reached the set temperature, wait 30 seconds, and then turn the steam line valve an 8th of a turn (45 degrees) to purge any water. Then fully open the steam line valve (quarter turn, 90°).
5. Close the front steam drain valve but leave the steam drain valve with steam trap open during testing.
6. Turn the superheater on with the VARIAC controller (on the back table by the DAQ box). Set the supplied power between 40-50% of full load. If the steam line needs to be drained at any point, immediately turn off the VARIAC controller.

7. Watch the steam temperature and pressure graphs on LabView to ensure that the steam temperature is rising. You may have to occasionally purge the steam through the front steam drain valve to get an accurate temperature reading (usually only once at the beginning will do).
8. When the steam temperature reaches 130°C, increase the steam controller setpoint to the desired steam saturation temperature (typically 162°C). Note: When the steam injection valve is opened, the temperature setpoint will have to be about 2°C above the desired temperature setpoint due to pressure losses in the steam line.
9. The steam line should be at or near the target saturation temperature before the steam injection valve is opened. The steam should already be superheated by the preheater, but during testing, it may take some time for steam purging to the drain before the temperature rises above the saturation point.

A.7 Collect Data

When testing you should make sure to monitor the water level in the deaeration tank via the tank level indicator in the lower left corner of LABVIEW. You will need to pause steam injection and testing when the level hits 2 gallons remaining to prevent starving the pump. Refill the deaeration tank from the backup tank and reheat it to 80 C before continuing. Also monitor the scale to ensure the bladder tank doesn't go above 120 lbs. When it gets close, stop injection and dump using the top drain valve (to help keep air out). Before testing:

1. Ensure that there are no air bubbles in the water loop and that the steam is at or above the target saturation temperature.

2. Ensure that the camera is set up correctly for data collection. Often you need to make some adjustments to the camera position during injection to make sure that it captures the entire plume. When finalizing the camera position:
 - Remember that when you are starting in the stable regime, the plume may not take up much of the frame, but this will change when it goes unstable.
 - Remember that once you have collected one data point at a certain camera position, all other data points must be collected from this camera position. Do not knock over the camera or try to readjust in the middle of a set of data.
3. Bring the loop to the correct starting process conditions by controlling each process variable using the following procedures:
 - Water Pressure: Adjust compressed air dial leading to bladder tank. The highest operating pressure we have used thus far is 75 psi.
 - Water Temperature: Adjust red electrically controlled valve that controls flow rate on the cold side of the heat exchanger. The valve position can be adjusted using the control block in the lower right of the LABVIEW code. Ensure the chilled water line is turned on at the top of the loop and at the water supply line by the pillar next to the annular flow loop. The water temperature is defined as the inlet temperature in the test section. Note: Do not let the test section outlet temperature get above 85°C at any point.
 - Water Flow Rate: Adjust the flow path valves, starting with the yellow valve between the heat exchanger and the air separator. Then adjust the blue valve after

the air separator, but before the water loop pump if necessary. The highest flow rate is about 17 gpm, but tests are typically done between 10 and 15 gpm.

4. SLOWLY open the steam injection valve to prevent a pressure spike that may damage the pressure transducers. The steam pressure must be above the water pressure to prevent water backflow into the steam.
5. If you notice significant air accumulation in the water side after opening the steam injection valve, close it, empty the steam line completely (turning off the preheater), reheat the water in the deaerator tank, and redo section A.4.
6. If you notice a spike in the steam mass flow rate on the order of grams, there is water trapped in the steam line. Open all drains leading from the steam side to purge out any condensate. The steam mass measurement trends should mirror the steam pressure and steam temperature trends. If the steam mass flow rate still seems off, see step 7.

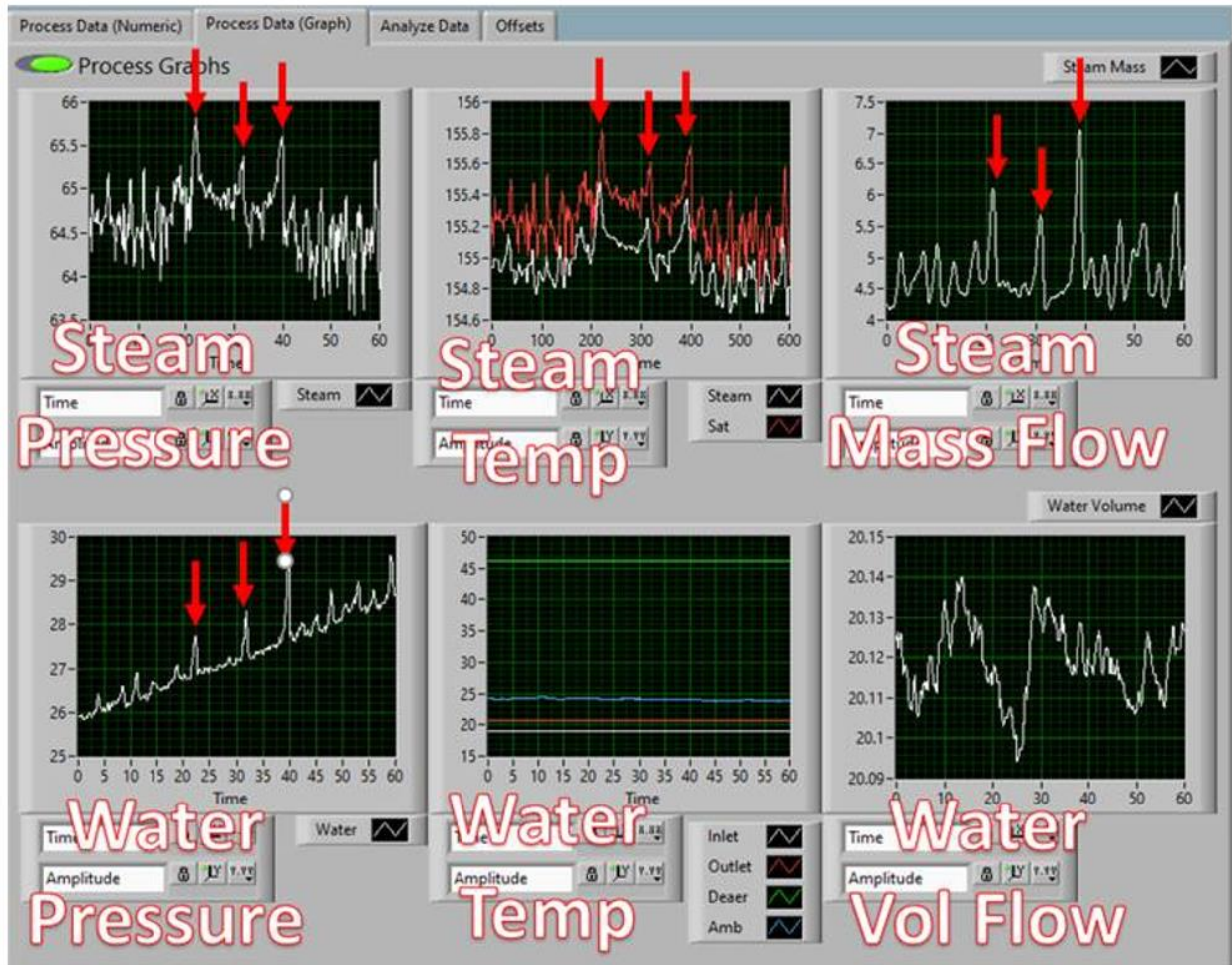


Figure A11: LabView front panel process data graphs with legend for each graph.

7. To control the test section inlet temperature, use the red HANBAY valve in LABVIEW to stabilize the process as much as possible.
 - Finely adjust the valve (in tenths or hundredths of a volt) to achieve a flat temperature slope, which is more challenging at higher temperatures.
 - Ensure the steam is superheated by monitoring for at least 1 degree above saturation, adjusting the VARIAC set point as needed (below 65% to avoid insulation damage).

- When the inlet temperature approaches the target within $\pm 1^\circ\text{C}$, click ‘capture’ on the PCC software to prepare the camera for data collection.
8. Change the trial to save box to name the data point accordingly, the naming convention for the nozzle is ‘NozzleNameTodaysDatePressureRatio’, e.g. 1CB110120PR056. Figure A12 shows a sample filled out trial save box.

Trial To Save	
Disk Drive Letter	E
Nozzle Type	1SE08025DPA
Steam Pressure	70
Water Pressure	34
Water Flow Rate	15
Water Temp	80

Figure A12: LabView file saving info for a sample nozzle.

11. Prep the r8080 software by clicking “play”. Then select “no” when asked to save the prior data point and set the data points to 20 at 0.5 s. When you hit your target temperature for the test, click “run”.
12. Once you have reached the target temperature, click ‘save data’ on the LabVIEW interface and THEN ‘trigger’ on the PCC software to collect the video. Figure A13 shows where the ‘save data’ and ‘trigger’ buttons are on each software.

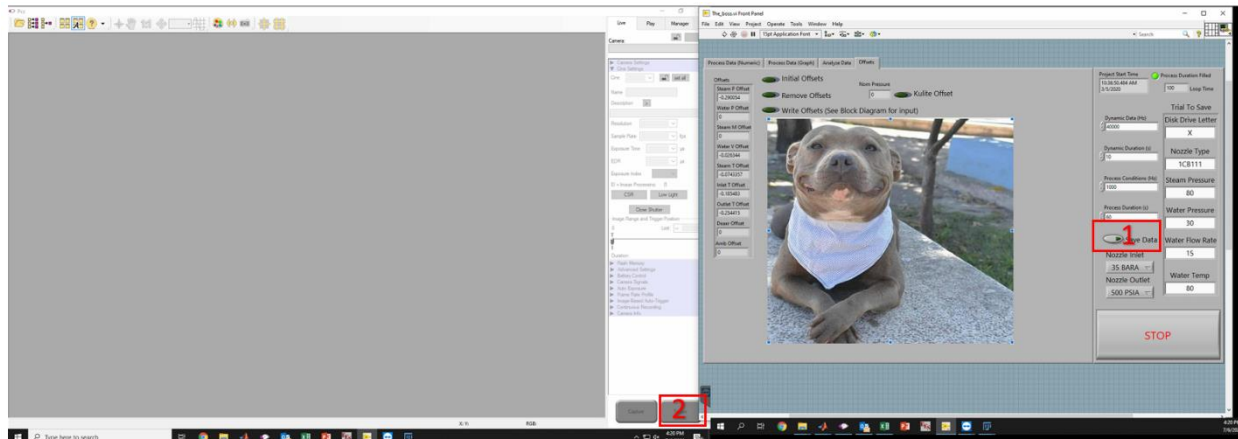


Figure A13: Location of trigger buttons to save data in PCC and LabView.

13. The LabView data saves automatically, but you must save the videos manually. Go the ‘play’ tab on PCC software and click ‘Save Cine’. You will be prompted to save it. Find the folder in which the process data has been saved, save the file with the naming convention: ‘NozzleNameTodaysDatePressureRatio-SteamPressure-WaterPressure-WaterFlowRate-WaterTemp’, e.g. 1S-80-30-15-70. Change the settings on the save file range to be ‘user-defined’ with a starting point of 0 and an ending point of 40,000 (see Figure A14) You will save it as a .cine file. Click save.

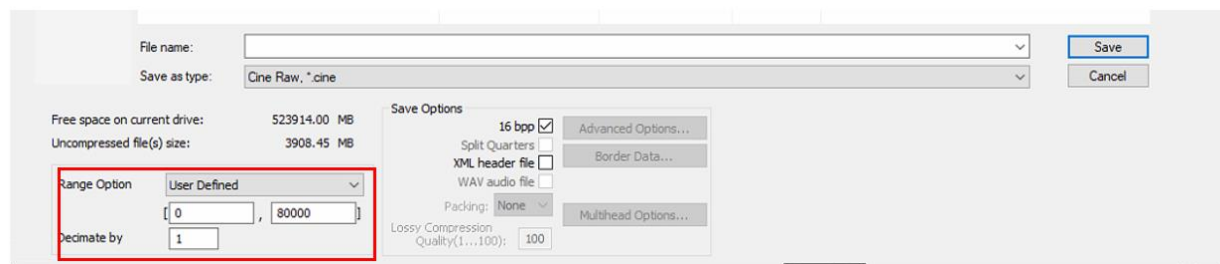


Figure A14: Location of range adjustment for saving cine file.

14. Save the r8080 data by clicking the save to file icon in toolbar. When prompted with a file name follow the convention: ‘NozzleNameTodaysDatePressureRatio-SteamPressure-WaterPressure-WaterFlowRate-WaterTemp-db’. Save the file in the same location as the

process data and cine file. When prompted with what points to save, select 'All' and then 'OK'.

15. Proceed to the next target temperature while the video is being saved to the associated hard drive. You may need to adjust the chilled water control valve to increase the temperature.

16. Repeat for all target temperatures (25 to 80°C in 5°C increments).

While running the tests:

- Consistently survey the loop to ensure nothing is leaking or broken.
- Check the water level of the deaerator tank and feed tank. Fill, as necessary.
- The bladder tank will fill up with water as you test. Once it has reached about 110 lbs, shut off the steam injection valve and bleed water out of the top drain valve on the water loop. This will prevent overfilling the bladder tank. If the loop is hot ($>80^{\circ}\text{C}$), turn on the chilled water to full open and stop injecting steam.
- When you have finished emptying excess water from the loop, it may need to be deaerated again. Do NOT adjust the camera to look at bubbles. Go by sight only.

A.8 Collecting reference pictures

When you are done collecting data but before cleaning up, a reference picture must be taken for the day to scale the video data. Complete the following steps to obtain the reference picture.

1. Do not adjust the camera.
2. Shut off any steam injection. Be sure the turn the valve slowly.

3. On the optical tray, slide the camera 20 mm forward from where it was focused on the nozzle to move the focus plane to the back window.
4. Take a video like you would for a data point (same camera settings) with the 0.1" grid paper in view on the back window.
5. When saving the video, change the file type to 'TIFF 16,48 images' and the range option to be 0,0 to save only a single reference image. Figure A15 shows the proper option in the dropdown menu.

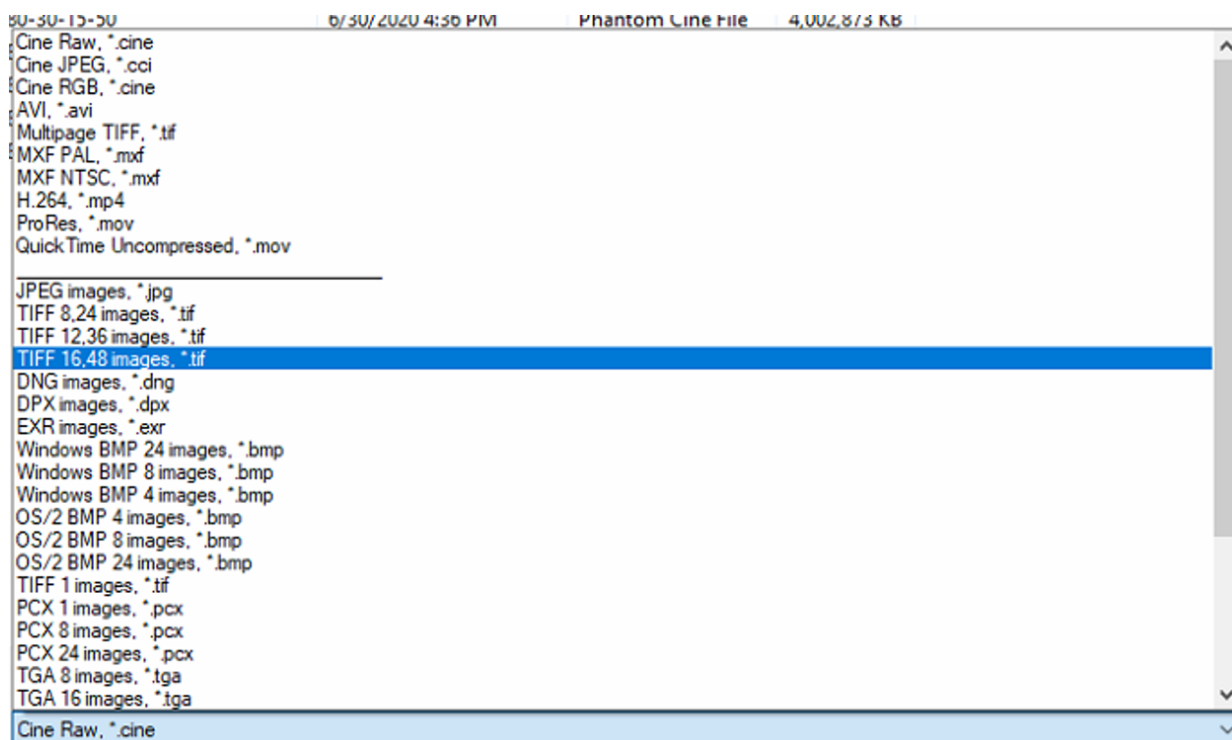


Figure A15: File save dropdown menu for saving the file type of the reference image.

6. The file name should be 'NozzleTypeTodaysDate-REF-Xdegbelow', e.g. '1S062520-REF' where the 'Xdegbelow' is the angle from level that the camera is angled down.

7. Once you have the reference image, also take a blank photo (no steam injection) while focused on the nozzle inlet port (you will have to slide the camera back 20 mm). As always, never adjust the lens, only the optical tray to adjust the focal plane. Save the image with the same naming convention as the REF image.

A.9 Loop Shutdown

1. Turn the preheater off by turning the VARIAC controller set point to zero and flipping the switch to the “off” position.
2. Close the steam injection valve and set the steam generator temperature to zero (do not turn it off).
3. Close the steam line feed valve (the valve most upstream from the nozzle on the steam line) to prevent any new steam from entering the line.
4. Vent the steam out of the system through the front steam drain valve.
5. Vent the steam out of the steam generator line by opening the yellow valve in the back by the deaeration tank injection valve. Do not leave this valve open. If it is left open, it will siphon water from the deaerator tank.
6. When the steam generator has reached 100°C, shut down the steam generator and turn off the 480 V breaker on the ceiling. (*This will take a while, proceed to the rest of shutdown while you wait*).
7. Turn off the water loop pump by shutting off the pump start switch and flipping the box disconnect switch off.

- Then, open the heat exchanger valve (the open valve at the bottom of the heat exchange).
 - Switch the three-way valve by the mass flow meter to direct water to the drain.
Open the top air valve to allow air to enter the loop.
8. Once most of the water has been emptied from the loop, open the top and bottom drain valves to get rid of any further water. You may want to open the compressed gas valve to push water out of the system, but close all vents open to the air if so. The scale on the bladder tank should read 65 lbs or less.
 9. Open all vents to the air except for those around the deaerator tank.
 10. Stop the LabView program and exit the software.
 11. Stop the PCC software and unplug the camera (power first, then other cables). Recap the camera and place the lens by the computer station in a noticeable spot.
 12. Gently bring the camera back to the pelican case in the side room along with all cables unless you know you will be the first one testing with it again.
 13. Unplug the 120 V extension cords leading to the outlet on the floor.

A.10 How to convert cine files to tiff for image processing

The following steps are meant to be a guide for converting 12 cine files from one test into a folder of tiff images that can be read by an image processing algorithm.

1. Reopen the PCC software and click the batch convert file button on the top ribbon, it will look like 3 tan files leading to 3 purple files as seen in Figure A16.

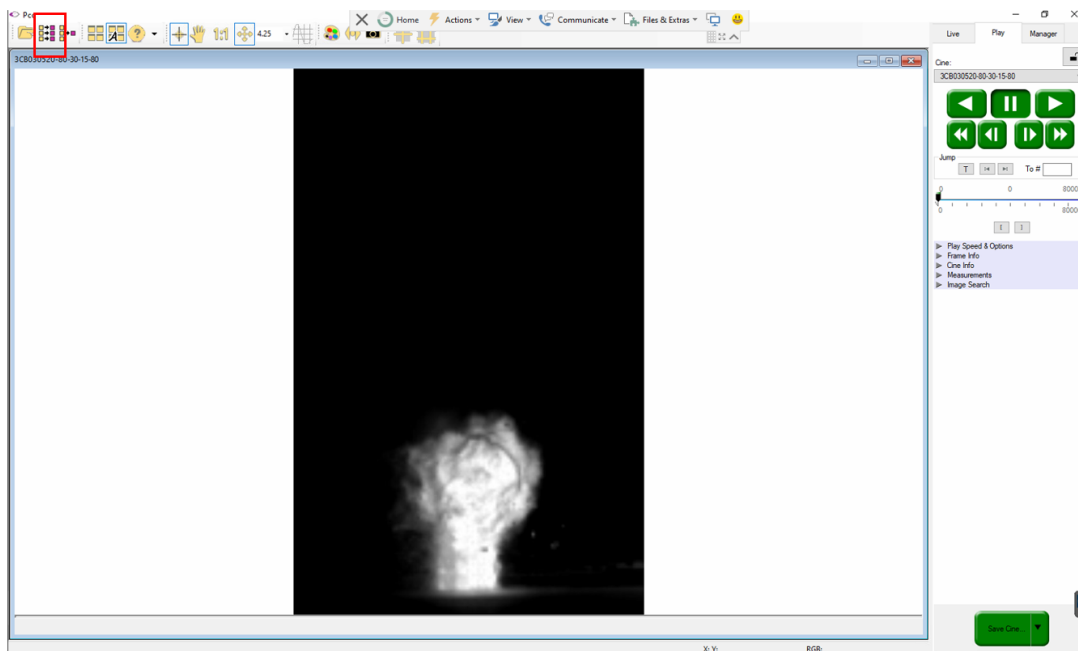


Figure A16: Location in PCC menu on the batch convert option in the toolbar.

2. Highlight all videos taken for the day and click open.
3. Under file name, type +5 and change the file type to be TIFF 16,48 images, the range will be the full cine. Click convert.

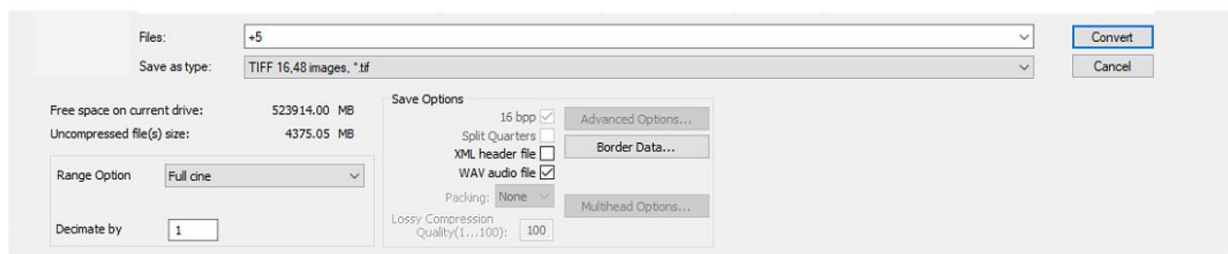


Figure A17: PCC save menu to batch convert all selected cines.

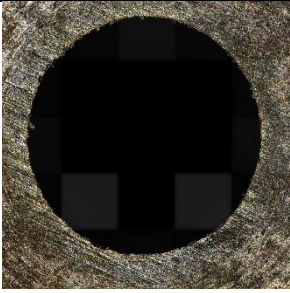
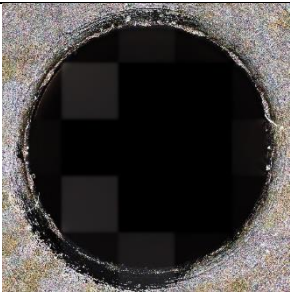
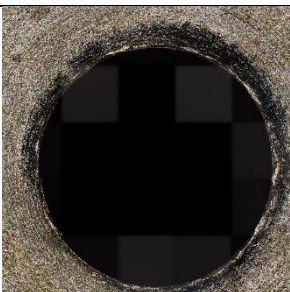
4. It will prompt that there are files in the folder, and they may be overwritten. They won't. Hit yes. Ensure that the software is processing the files into tiffs, you will see a status bar on the screen.

5. Turn off the computer monitors, but do NOT turn off the computer. The files will be converted overnight and ready for further processing in the morning.
6. Revisit step 6 from A.9. Do not leave until the steam generator has cooled to 100°C or less and you have turned off the 480 V breaker on ceiling.

Appendix B: Nozzle Geometry and Scans

The LEXT-3D confocal laser scanning microscope was used to evaluate the nozzle outlet profile. This tool enabled much higher resolution imagery and the ability to quantify features compared to the previous method of X-ray scans. Scans of each nozzle used in this work are provided in Tables B1 – B3 below.

Table B1: Length to diameter ratio study nozzles.

Nozzle Image	Nozzle Name	Measured Diameter (in)	Manufacture Date & Shop
	1SE	0.0948	Feb. 2023 Roberson Tool
	3SE	0.0970	(Not certain, but believed to be:) Q1 2023 Roberson Tool
	6SE	0.0953	(Not certain, but believed to be:) Q1 2023 Roberson Tool

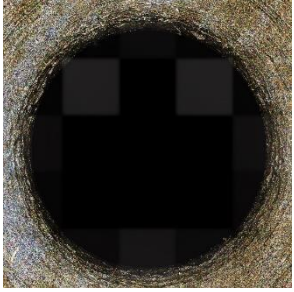
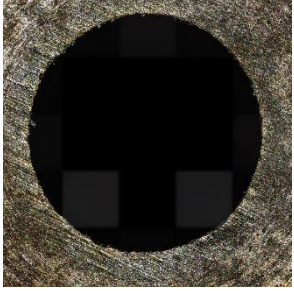
	8SE	0.0958	Feb. 2023 Roberson Tool
---	-----	--------	----------------------------

Table B2: Diameter study nozzles.

Nozzle Image	Nozzle Name	Measured Diameter (in)	Manufacture Date & Shop
	1SE0.065	0.0672	Feb. 2023 Roberson Tool
	1SE0.080	0.0813	Feb. 2023 Roberson Tool
	1SE0.096	0.0948	Feb. 2023 Roberson Tool
	1SE0.110	0.116	Feb. 2023 Roberson Tool

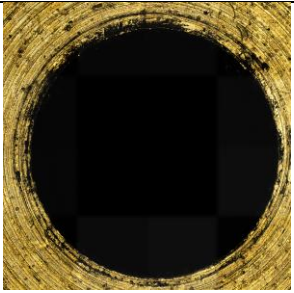
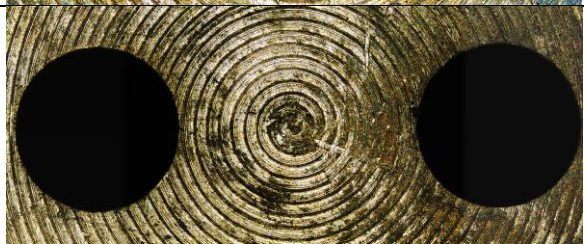
	1SE0.125	0.128	Feb. 2023 Roberson Tool
	1SE0.065 NEW	0.0657	Oct. 2024 AlphaWireEDM LLC
	1SE0.080 NEW	0.0797	Oct. 2024 AlphaWireEDM LLC

Table B3: Dual-port study nozzles.

Nozzle Image	Nozzle Name	Measured Diameter (in) (S= Spacing)	Manufacture Date & Shop
	1.5D 0.080	L:0.0806 R:0.0809 S:0.120	Sept. 2023 AlphaWireEDM LLC
	2.5D 0.080	L:0.0810 R:0.0811 S:0.200	Oct. 2023 AlphaWireEDM LLC
	3.5D 0.080	L:0.0820 R:0.0816 S:0.280	Sept. 2023 AlphaWireEDM LLC
	1.5D 0.065	L: 0.0660 R:0.0662 S:0.0970	Oct. 2023 AlphaWireEDM LLC
	2.5D 0.065	L:0.0662 R:0.0663 S:0.1625	Oct. 2023 AlphaWireEDM LLC
	3.5D 0.065	L:0.0660 R:0.0660 S:0.2273	Oct. 2023 AlphaWireEDM LLC

Appendix C: Lighting and Imaging Changes

Initial high-speed videos were taken with a Fiber-Lite MI 150 light with a 150-watt halogen bulb. The plumes were illuminated from the front, which resulted in an image like Figure C1, where the plume is white and the background is black. The old footage was recorded at 80,000 frames per second with a 128 x256 resolution and a 12 μ s exposure time with the Phantom v311 camera and a Nikon Micro-NIKKOR 55mm lens.

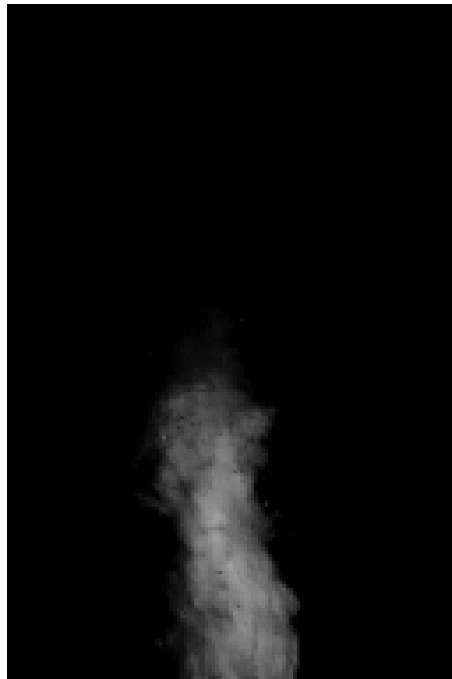


Figure C1: Sample image of steam plume from a front-lit setup prior to lighting/imagery changes.

The back of the test section viewing window was a stainless-steel plate of the same dimensions as the front quartz glass window. The back plate was used in prior studies by Zach Alden to measure pressure fluctuations near the steam plume. This plate was painted black to prevent reflections from a raw stainless-steel plate. Because a pressure transducer had to be attached to the plate, a 5/32 inch threaded hole was machined into the center of the plate (Figure

C2). Christian Thorpe used this hole to determine the pixel size, but his method did not bring the port into focus, so there was uncertainty in the pixel to inch conversion.



Figure C2: Sample reference image of the old pressure transducer port used to calibrate images for image processing.

In this work, we changed the lighting and calibration approach so that we could more easily measure the plume penetration depth. The first step to overhauling the lighting setup was to replace the stainless-steel backing plate with a quartz window (identical to the front window). A new light was needed as the gooseneck Fiber-Lite unit was not powerful enough to evenly light the whole test window. A mounting arm was added to the back of the test section to secure a new light, as shown in Figure C3. Once the mounting arm was installed, several lights were evaluated on image quality. First, several inexpensive LED panels were bought from Amazon, but they all flicker so they could not be used with the high-speed camera. After this first set of lights were evaluated, we bought lighting specifically built for high-speed video recording to avoid issues with flicker.



Figure C3: Boom arm to hold backlight and REED 8080 sound level meter.

First, we evaluated the MicroBrite BT 050050 as shown in Figure C4. This light was powered by a variable DC power supply found in the lab. The 50 mm x 50 mm MicroBrite LED light was large enough to illuminate the whole window and showed more of the plume than the front light format (Figure C4b). This added view exposed the issues of deaeration which prompted some operational changes to the loop described in Appendix D. One notable drawback to the MicroBrite unit was that it had to be used with a relatively high exposure time, meaning that intricate details on the plume surface and edges were lost. The second drawback was that it could not be easily mounted to a heat sink.

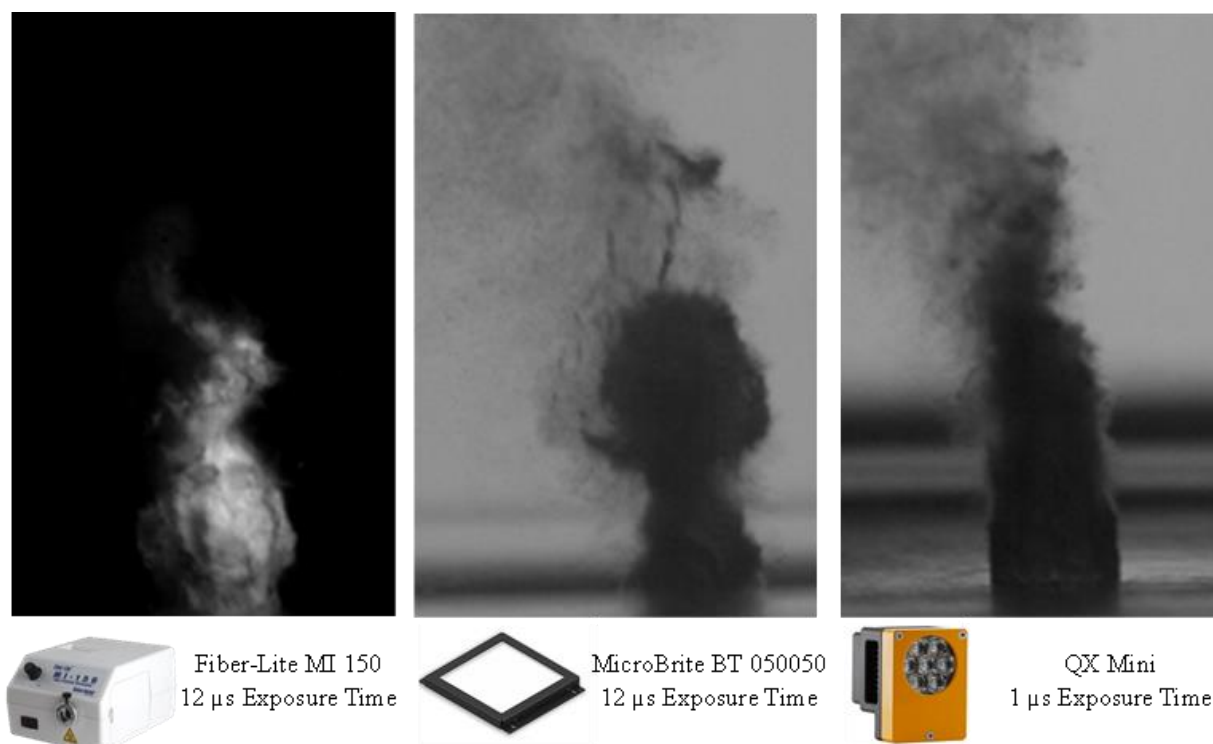


Figure C4: Evolution of lighting equipment with corresponding images. From left to right: original lighting setup, first back lighting setup after changing back plate to quartz, final backlighting choice.

To address these issues, the GS-Vitec QX Mini was tested on loan from the Phantom camera sales representative. The QX Mini is much brighter than the MicroBrite unit and has an integrated active cooling system, so it does not overheat. After testing the unit, it was bought and installed on the boom arm. The same DC power supply as the MicroBrite light is used to power the QX Mini, where the voltage controls the brightness. It is set to 30 V (the brightest setting) for all images shown in this thesis, and is only turned on for the few seconds of recording and is then shut off. At this brightness, the exposure time on the Phantom v311 is lowered to 1 μ s for enhanced details in the image (Figure C4). Some diffuser paper is taped to the face of the QX Mini to spread out the light evenly across the window and to prevent the seven individual LEDs from being visible in frame.

The most up to date lighting setup is a combination of the QX Mini (backlight) and the original Fiber-Lite M150 (front light). The front light was added to add definition to the front steam/water interface. Figure C5 shows a sample image with both lights on. With this setup, we significantly reduced the shutter speed and found that a framerate of 40,000 fps was sufficient to resolve the plume. The lower framerate allowed us to increase the resolution to 256 x 256 pixels, increasing the field of view compared to Figure C4. This resolution is helpful because some of the unstable plumes extended beyond the original capture window.

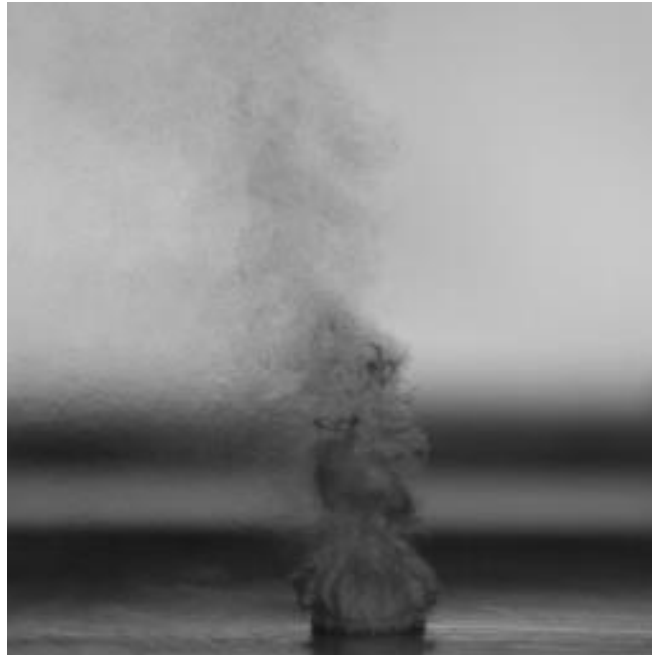


Figure C5: 256 x 256 steam plume with both QX Mini backlighting and Fiber-Lite M150 front lighting.

Since the back plate was removed and the pressure transducer port was no longer in view of the camera, a new method for capturing a reference image was needed. As stated above, prior reference images did not keep the reference object in focus, which creates uncertainty in scaling the images. To fix this, two perpendicular optical trays were affixed to the camera tripod with the v311 mounted on top of them. This allows for the focus plane of the camera to “truck” left and

right, and “dolly” toward and away from the test section. The dolly tray shown in Figure C6 is limited to 40 mm of total movement which is just enough to move the focal plane approximately 20 mm from the center of the test section (plume position), to the outside face of the rear glass window. Moving the camera along this axis enables the same focal length used during video recording to be used in the reference image capture. By holding a piece of graph paper between the QX Mini and the glass window, an in-focus calibration image is taken. The full procedure for taking a reference photo is described in Appendix A. A reference image from this updated method is shown in Figure C7.



Figure C6: Dolly optical tray at its furthest setting as dictated by the set screw to attach it to the truck optical tray below it. Test videos are taken at a setting of 20 mm, then the camera moves forward for the reference image.



Figure C7: New reference image with 0.1 inch square graph paper used as the calibration target.

Appendix D: Deaeration Procedure Overhaul

Micro air bubbles have consistently been an issue for the steam injection facility. The bubbles have caused issues for past students' image processing routines and have an impact on noise level. As of joining the project in April 2023, the deaeration procedure was both not reliable and exceedingly time intensive (taking up to six hours in some cases). In addition, switching to a back lighting setup worsens the issue by making all micro bubbles visible in the field of view, instead of just the ones that passed in front of the plume in the front lit era. Switching to back lighting made evident how much a full deaeration solution was needed.

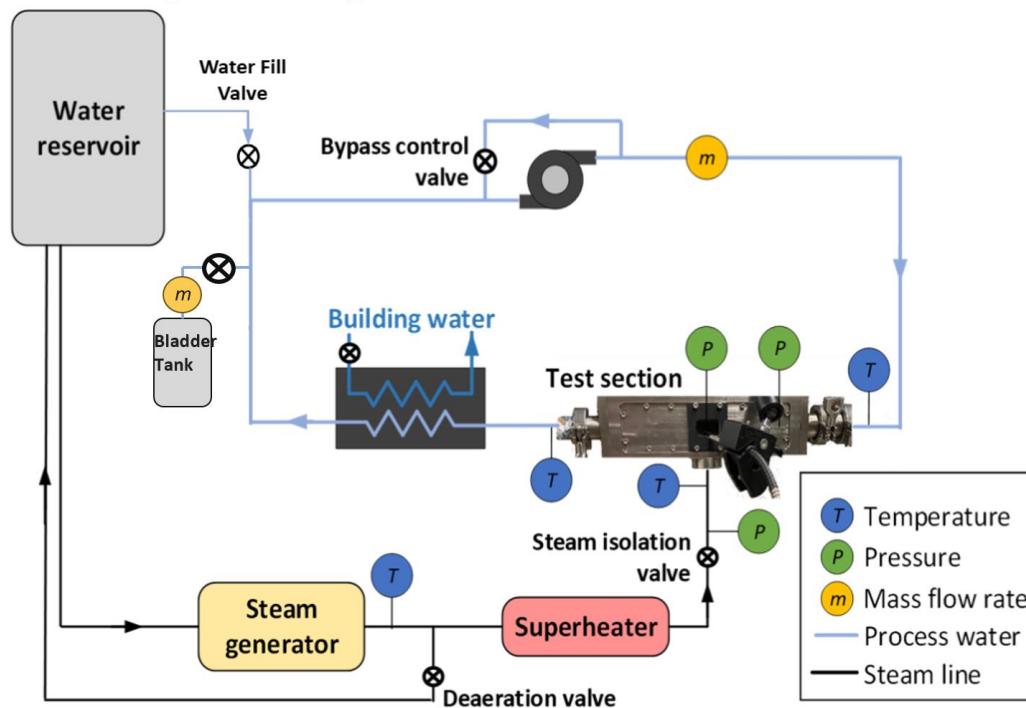


Figure D1: Steam injection test loop schematic as of April 2023.

Figure D1 shows a schematic of the loop when I joined the project. The first attempt at implementing a new deaeration solution involved installing a four-way diverting valve just after the water loop heat exchanger. Figure D2 shows a schematic of the loop with the diverting valve,

along with a photograph of the installed valve. The purpose of the diverting valve was to cycle process water through the open deaeration tank to allow microbubbles to float upwards and escape to atmosphere. Water from the loop would directly plumbed into the sidewall of the deaeration tank and then pulled from the bottom of the tank directed back into the main loop. The black steam feed pump was used to cycle the water with the manual override switch.

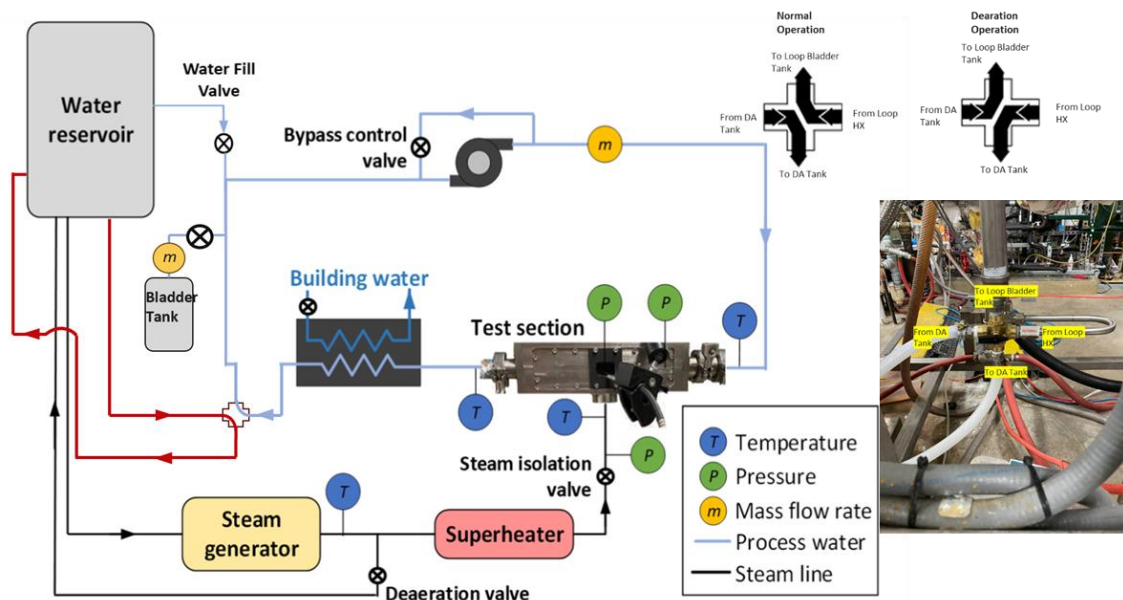


Figure D2: Steam injection test loop schematic with installed four-way switching valve. During normal operation the water loop is isolated, during deaeration, process water passes through the deaeration tank.

The diverting valve was sourced from McMaster Carr and had $\frac{1}{2}$ " NPT connections. After installation, we found that the pressure drop was too high, limiting the maximum flow rate of the water side of the loop to 2 gpm, down from 17 gpm. This limitation clearly was not a workable solution to the deaeration problem since it compromised the loop's ability to reach prior test conditions, and it did not show promising reductions in the volume fraction of air in the test section.

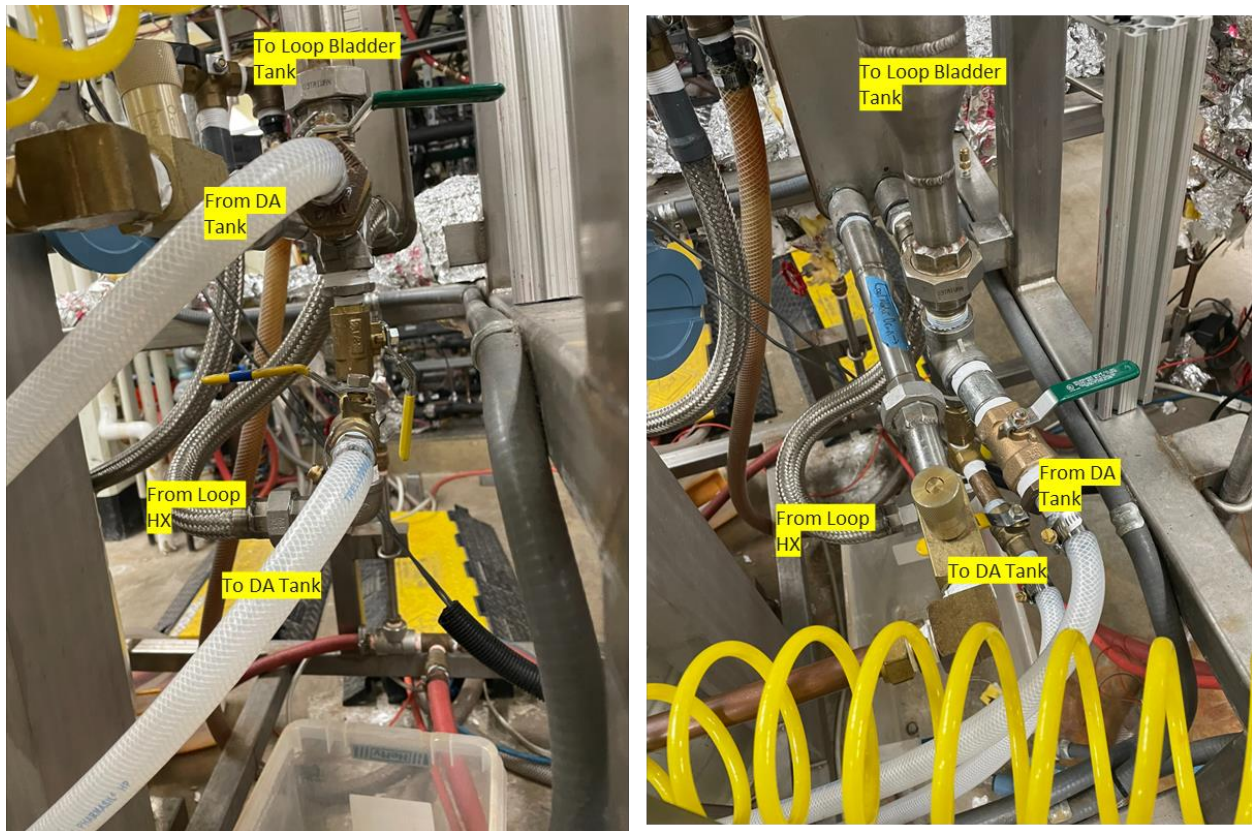


Figure D3: Two views of the deaeration valve manifold installed in the same location as the four-way valve, but with larger auxiliary plumbing to reduce pressure drop.

To fix the pressure drop issue, the four-way valve was replaced with the valve manifold shown in Figure D3. The manifold could send water to the deaeration tank during deaeration, and then isolate the tank during normal operation. Water from the deaeration tank was cycled through the test section at 80 °C using the steam feed pump with the manual override switch. This was done after the water side of the test loop was first filled to +5 lbs on the bladder tank weight. Pumping the water around the loop and through the deaeration tank was evaluated for different time intervals (15 to 45 minutes). No length of time was effective at removing air bubbles from the test section, as they would reappear in the test section in minutes after changing the manifold back to test operation. Additionally, although this iteration lessened the pressure drop in the water side of the system compared to the four-way valve, it was still significant enough to limit the

maximum water flow rate to 12 gpm (below the 15 gpm target). The method of routing the water through the deaeration tank during the deaeration phase was abandoned after this modification attempt.

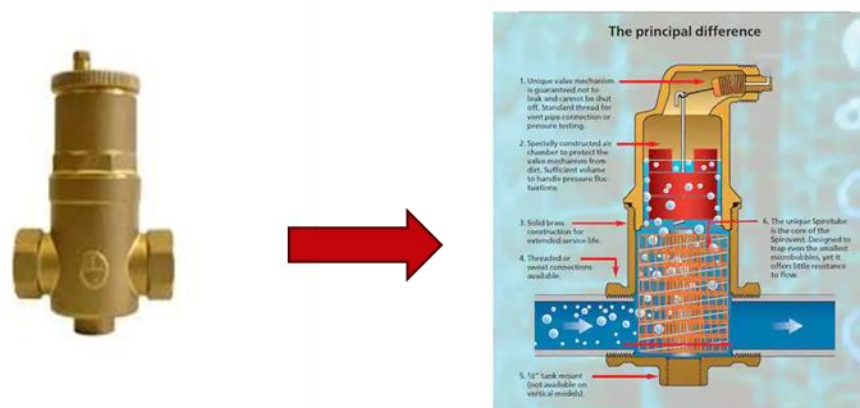


Figure D4: Previous air separator (left, Bell and Gossett EASB-Jr) and new passive air separator (right, Spirotherm Spirovent-Jr).

The next round of modifications focused on the existing air separator. As of joining the project in Spring 2023, the passive air separation unit was a Bell and Gossett EASB-Jr found at the outlet of the process water from the heat exchanger. The separator had an outlet on the bottom face where condensed steam passes through the mass flow meter before ultimately stagnating in the bladder tank. The EASB-Jr, shown in Figure D4, did not appear to allow air to escape from the top vent as no sound was heard in any prior experiments. At the top of the EASB-Jr, there is a cap for the air vent which was removed to allow for venting of air. Even with this cap removed, there was no noticeable volume of air escaping at any interval from the unit. The unit was then taken apart and the internals were inspected. It became clear that the unit was dysfunctional as the float which controls the air vent valve was not properly connected therefore preventing the valve actuation.

A new air separator unit was installed in the same location to fix the valve issues. The new unit is a 1-1/4" Spirotherm Spirovent-Jr, which was installed along with new auxiliary plumbing at the unit's water inlet, water outlet, and condensate drain. To accommodate the larger plumbing, the deaeration tank manifold was removed and replaced with a flex hose. A pipe cross was installed at the highest elevation of the heat exchanger exit and air separator inlet. A new manually actuated air bleed port was installed on the top of the cross and a pressure gauge was installed on the remaining side port of the cross. With these two additions, debugging of the new air separator and testing new deaeration techniques were both possible. The Spirovent-Jr was immediately effective at passively removing the non-condensable air in the process water. For example, while filling the process water loop, air audibly escapes via the air vent at the top of the passive deaeration unit. Venting is also now heard at random intervals while testing when enough air collects in the unit.

Finally, multiple permutations of valve opening and closing were attempted during both loop filling and isolated water cycling with no steam injection. In doing so, it was found that the water recirculation valve, which was used at the time to control process water flow rate, was adversely impacting the deaeration process. Aerated water was getting trapped in the recirculation loop and would occasionally send large volumes of air bubbles toward the test section, even after the loop was deemed deaerated for hours. The solution was to keep the recirculation path fully open during the fill and then closed during normal testing. A new inline ball valve was installed just below the pipe cross after the heat exchanger to control the process water flow rate.

Although the changes above resulted in a dependable deaeration procedure for system preparation, we often found that halfway through testing a nozzle; significant amounts of air would reappear and prevent the test from finishing. After further investigation, we found that closing the steam line allowed the air bubbles to dissipate within a few minutes. When injecting the steam

again after deaerating, the bubbles would reappear. An extensive leak test was conducted to figure out if air was entering the steam line downstream of the deaeration tank, but no leaks were found. Thus, the deaeration tank was identified as the source of the air.

The deaeration tank is normally heated to 80 °C to release any dissolved air prior to filling the water side of the loop. As water was removed from the tank, room temperature reverse osmosis filtered water from the buffer tank replaced it via a small pump controlled by a float level switch attached to the lid of the deaeration tank. The buffer tank was then filled by a normally closed solenoid valve activated based off another float switch at the top of the buffer tank. Constantly replacing the 80 °C water originally in the deaeration tank with room temperature water from the buffer tank rapidly lowered the temperature of the water, increasing the potential amount of air that could be dissolved in it. To address this issue, the float level switch in the deaeration tank was removed and the pump was rewired to be actuated by a manual switch, meaning the deaeration tank would empty throughout the test. Decoupling the deaeration and buffer tanks resulted in an issue with buffer tank filling. To resolve it, the buffer tank solenoid valve and float level were rewired so that the buffer tank is always trying to fill to the top, not only trying to fill as the deaeration tank level decreased. This was crucial because the flow rate of water from the reverse osmosis filtration system is on the order of 0.5 to 1 gallon per hour while a DCC test can use 5-12 gallons of water. The most effective method of achieving loop deaeration is described in Appendix A and can be accomplished in ~15 minutes.

Future improvements to the deaeration process might include installing a vacuum pump to remove the large volume of air present before water is added to the loop. This may not be possible due to the sanitary fittings throughout the piping and instrumentation that is not explicitly rated to handle vacuum. A reliable method for measuring the volume fraction of air in the water could also

assist in the deaeration process. Image processing through the test section window could be used for this purpose, although this has not been systematically evaluated.

At the end of each testing day, water is drained from the loop because attempts at moving the deaerated water in the bladder tank back to the deaeration tank resulted in re-aerating the process water. This dumping results in the current time-limiting step which prevents running many tests in the same day. Since the deaeration tank must be refilled with filtered water from the buffer tank (not water from the loop), the volume of the buffer tank sets the total amount of water that can be used in one day of testing, and the flow rate of the reverse osmosis system sets the downtime between test sets. Currently, the buffer tank holds approximately the same volume as the DA tank. Depending on the nozzle, the DA tank may need to be completely refilled between tests, limiting testing to two cases per day. Alternatively, a higher throughput filtration system could be employed to refill the buffer tank, or a larger volume of buffer could be installed to have more filtered water on hand (although more time would be needed between testing days to refill that tank).

Appendix E: Chilled Water Needle Valve Improvements

The main parameter that we actively control during an experimental run is the process fluid inlet temperature. The temperature is controlled by adjusting the chilled building water flow rate through the cold side of the brazed plate heat exchanger. The flow rate of chilled water was initially controlled using a manual needle valve at the exit of the cold side of the heat exchanger. Between each data collection point (for example, 30 °C to 35 °C), the test operator would leave the data monitoring station to slightly close the valve and reduce the cooling water flow rate. This in turn would increase the process water temperature. There were three issues with this approach. First, the operator needed to leave the test computer, both a safety concern and an inconvenience. Second, the needle valve was oversized and only operated in the bottom ~10% of the range, meaning that small changes in the valve position ($1/16^{\text{th}}$ of a turn or smaller) resulted in large changes to the process water temperature. Lastly, the valve could not be automated to achieve a target temperature as set by the operator. More information on each issue is provided below.

Moving back and forth between the computer and the valve means the operator does not get instant feedback. If the valve is closed too far, the process water temperature will rise too fast for the next data point to be taken. Missing the setpoint temperature not only wastes time, but also wastes water given the new deaeration tank setup (see Appendix D). The largest diameter nozzles use ~10 gallons of water over the course of the experiment, meaning there is not much margin for error with a tank capacity of 13 gallons. To avoid overshooting, the operator had to make minor changes to the valve position and then go and look at the LabView screen to see the effect. This would happen many times for each data point until the target temperature was reached.

Additionally, the oversized valve caused issues with hitting the proper setpoint, especially at the end of the experiment ($T_{\text{in}} = 80^{\circ}\text{C}$). For this condition, the valve was nearly closed and any

adjustments were difficult as the valve would stick near the bottom of the range. When it did move, it would often turn more than the operator intended and end up overshooting the target temperature. Additionally at these elevated temperatures, the valve body was too hot to touch without wearing thick steam gloves, again making it more difficult to precisely turn.

Finally, the manual valve prevented the use of an automated control scheme. An automated valve could alleviate the issues described above and introduce repeatability into temperature control between tests. By manually adjusting the valve at each data point, there is variability between temperatures on the rate of change of temperature. Introducing a PID controller could make the temperature and slope of temperature consistent, giving more confidence in our data.

To address these issues, a Hanbay MCM-050AF-3-SS-8GUF8 electrically actuated needle valve was purchased and installed to replace the manual needle valve. The actuator connects via a 5-wire cable to the DAQ module and a DC power supply. Table E1 shows the functionality of each wire. The output signal (Grey wire) is not currently utilized but can output a signal indicating the percent opening in real time (useful for feedback control). A variable DC power supply was used to supply the +24 V power to the controller. The voltage control signal is provided by the NI MOD #9263 card and is read into LabView.

Table E1: Hanbay needle valve controller wiring functionality.

Wire Color	Wire Function
White	+24 VDC
Black	Power Gnd.
Gray	Output Signal (if applicable)
Brown	Input Signal Gnd (isolated if applicable)
Blue	Input + Signal (isolated if applicable)

The actuated valve was integrated into LabView by slightly modifying a LabView PID w/ autotuning example. The control scheme was designed to be flexible, allowing for (1) manual control, (2) PID control via manual gains, and (3) PID control via autotuned gain. Currently, the Hanbay valve is manually controlled, meaning the operator must decide what voltage to send to the controller which translates to a percent open of the needle valve. From initial testing, only voltage signals between +1 to +3.5 VDC are needed to cover the full range of test temperatures. The controller can safely handle control signals in the range of +1 to +10 VDC, where 1V is fully closed and 10V is fully open.

An extra thermocouple was added to the process water outlet stream of the heat exchanger and will be used as the control signal for the Hanbay valve. The thermocouple was added because we found that controlling from the test section inlet temperature introduced too much lag in the system. There is a small temperature difference between the heat exchanger outlet and the test section inlet due to losses along the piping, but it is negligible when trying to reach a steady state temperature for testing.

Tuning the PID controller has been challenging. While moving the control variable to the outlet of the heat exchanger helped, we have not found the right gains. Basic trial and error has shown that the P gain needs to be negative to avoid driving the temperature away from the setpoint and that a PI only controller seems to be advantageous compared to a PID controller given the added complexity of the derivative value. The task of finding correct gains for the controller is complex given that each nozzle has a different steam mass flow rate resulting in different heating loads. Our work shows that the gains should be a function of the steam flow rate. There are two plausible paths for future work on the steam loop to get the PID controller to operate. The first is to fully investigate the autotuning feature and improving the logic so that regardless of what nozzle

is in the loop, LabView can autotune the gains in a few minutes before collecting data. Note that autotuning was unsuccessful when implemented for the annular flow loop so it likely not a viable path. The second route is to manually map out each nozzle/mass flow rate of interest and find what gains work for each nozzle. This data would then be used to make a lookup table for the operator to select what gains are needed based on the nozzle. The latter strategy is planned alongside an overhaul of the LabView code in the coming semester.

Appendix F: Steam Superheating Changes

F.1 Replacing the Rope Heaters

Steam superheat was initially controlled by a temperature control unit which switched the preheater on or off based on outer pipe wall temperature at the preheater exit. The controller allowed the user to select a temperature setpoint and deadband and would provide 120V AC power to the heater unit when the measurements were below of the lower deadband limit. The preheater consisted of three electric resistance rope heaters, shown in Figure F1. A junction box connected the rope heaters in parallel to the power source. The junction box was initially suspended in the air below the steam pipe and held by the heater wire leads (Figure F1). This was an obvious safety concern as any leak of water from the piping above could short the heaters.

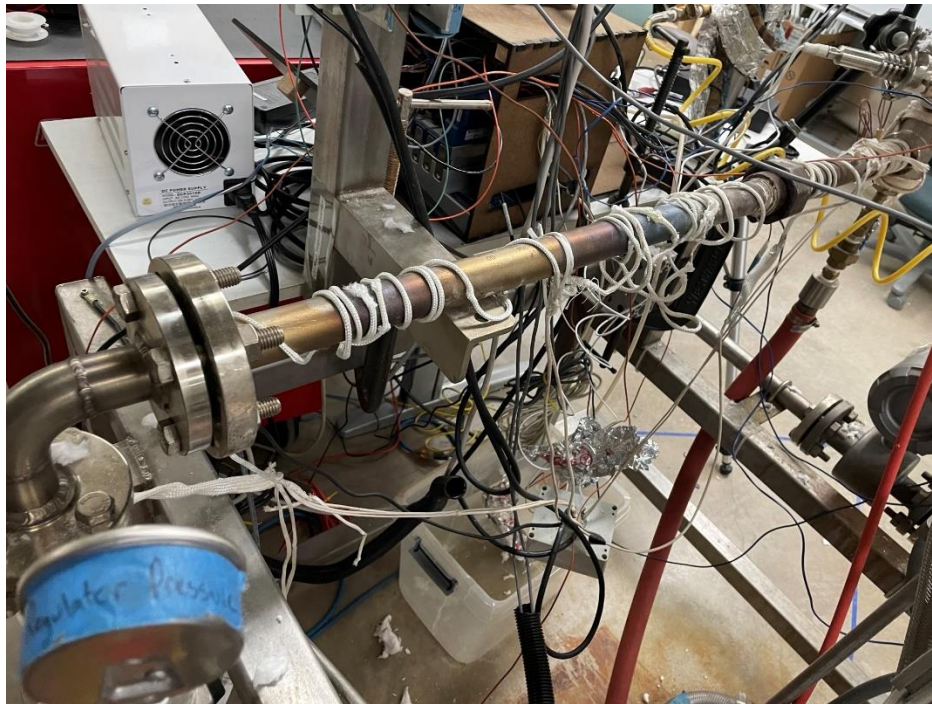


Figure F1: Original rope heaters used to superheat the steam a few degrees Celsius.

The rope heaters themselves were a mess underneath the pipe insulation. Each of the three rope bodies were wound loosely around the steam pipe, which may have resulted in overheating due to poor thermal contact. Additionally, the woven sheathes were frayed and the heating wire was exposed some locations, again a fire hazard. There also was not an even distribution along the heated length which led to corrosion on the pipe surface (another sign of overheating). The main goal of a new superheating system were to address these safety concerns, and to transition away from an on/off controller to prevent cyclical thermal stress on the plumbing.

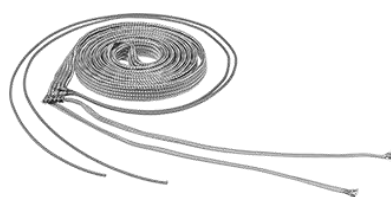
To address these issues, we first removed the old rope heaters and electrical control box. The temperature control module was unwired and returned to the lab's surplus on the East wall of the MFVAL lab. A VARIAC transformer (Figure F2) was purchased from McMaster-Carr and installed in the same location as the previous temperature controller. This unit was selected because it can supply a constant voltage to the new heaters, and therefore a constant power. It was then plugged into the same extension cord the DAQ module is powered by. The wire that used to provide power to the junction box was then plugged into the VARIAC.



Application	Power
Transformer Type	AC to AC
Transformer Voltage Function	Step Up/Step Down/Constant
Electrical Phase	Single
Voltage	
Input	120V AC
Output	0V AC-140V AC
Power Output	1,400 VA
Maximum Current	10 A
Connection Type	
Input	Plug
Output	Socket
Input Plug Type (NEMA Style)	Three Prong (5-15)
Input Cord Length	6 ft.
Output Socket Type (NEMA Style)	Three Slot (5-15)
Frequency	50/60 Hz

Figure F2: VARIAC power controller for the superheating wrap.

Next, a new heater was sourced from McMaster-Carr to replace the frayed rope heaters. The new heater is shown in Figure F3. It was chosen for its high operating temperature limit and Watt density. An energy balance on the steam with the highest mass flow rate (~ 6 g/s) and lowest gauge pressure (70 psi) showed that only 30 W is needed to superheat the steam 2 °C. One heater rated at 624 W is more than enough to supply the desired superheat under steady state conditions even with losses to ambient. The selected heater was wound carefully around the steam piping to avoid overlap, which can result in overheating and fraying. Insulation was then wrapped around the piping with the heat rope to provide good thermal contact and minimize heat losses.



Heater Type	Cable
Heat Cable Type	Constant Wattage
Length	8 ft.
Wattage	624 W
Watt Density	78 W/ft.
Voltage	120V AC
Electrical Phase	Single
Current	5.2 A
Width	1/2"
Thickness	1/8"
Temperature Control Type	None
Maximum Heat Output	1400° F
Environment Temperature Range	-60° to 1400° F

Figure F3: Rope heater controlled via VARIAC to superheat the steam. Relevant electrical information from the supplier is shown.

The superheater is only rated up to 120 VAC, but the VARIAC is capable of supplying 140 VAC meaning the VARIAC should never be operated above $\sim 85\%$ of full power. Given that only 30 W of heat are needed to superheat anyway, there is no need to exceed 60% of full power even if there are substantial losses. At 60% and above the insulation can be at the risk of burning, which has a noticeable smell. An example of small burn marks on the insulation are shown in Figure F4. If burning insulation is ever smelled, turn down the heater power 10%.



Figure F4: Photos of opened insulation after the initial runs with the new preheater (October 2024). The burns are only on the closest layer of insulation and don't extend further.

F.2 Replacing the Steam Temperature Sensor

Steam process parameters (pressure and temperature) are measured just below the test section, but upstream the steam injection valve so that they can be checked prior to injecting. Originally, a cast iron reducing tee was used to mount the dynamic pressure transducer and the thermocouple used to measure the process parameters in an offshoot of the main flow path as shown in Figure G1. The cast iron fitting was replaced at the same time as the superheater changes and is described in Appendix G. The original temperature sensor was measuring a relatively stagnant pocket of steam off of the main flow path. The pressure transducer was fine in this location but the temperature sensor was moved to better capture the bulk fluid temperature entering the nozzle.

The first attempt at moving the temperature sensor is shown in Figure F5. A tee was added so that a long thermocouple could be placed in the center of the main steam flow path. A 12" type T thermocouple was sourced from McMaster Carr and installed into the assembly. One immediate issue with this orientation was that steam trapped in the added tee would lose heat to the

surroundings and condense. The condensed liquid water would then buildup on the membrane of the pressure transducer. The droplets would bounce on the pressure transducer's membrane and result in data with high amplitude noise. This problem was solved by rotating the added tee 180 degrees, so the pressure transducer was mounted on the top of the assembly.



Figure F5: New tee fitting installed to allow for direct measurement of steam flow temperature. A 12" type T thermocouple was used to measure the steam temperature.

The next issue with this setup was inaccurate temperature measurements. Seemingly random spikes in temperature would come in waves and last for a few minutes before plummeting back down. After removing the test section to replace a nozzle, it was clear that the thermocouple was touching the wall of the main flow and not suspended in the center of the flow path. Backing out the thermocouple so that it would measure at the proper location did not fix the issue. It did remove the temperature rises but not the drop-offs. The likely explanation for the measured temperature dropping (and dropping enough that the temperature was below saturation temperature) was that liquid condensate built up in the volume of the measurement tee, then would

flow back into the main channel. This condensate had plenty of time to cool in the uninsulated piping to be below the saturation temperature.

The measurement assembly was removed from the loop and the tee in the main steam path from Figure F5 was replaced with a $\frac{3}{4}$ " stainless-steel cross. One leg of the cross now accommodates the pressure transducer and the other leg holds the thermocouple. Figure F6 shows the new steam sensor setup. This solution allowed for relatively easy adjustments to the thermocouple to ensure it was no longer touching a pipe wall. There have been no issues with condensate buildup after going to this smaller volume assembly and insulating it.



Figure F6: Insulated cross installed for the steam process parameter measurement as of December 2024.

Appendix G: Rusted Fitting

In Spring 2024, a small steam leak was noted just below the test section. This leaking steam condensed into the “dynamic” microphone’s membrane and broke the device. The source of the leak was investigated by removing the insulation around the test section steam injection valve and it was discovered that the tee holding the dynamic pressure transducer was rusted (Figure G1).



Figure G1: Rusted fitting that had a steam leak. The fitting was crumbling at the touch and an immediate replacement was needed.

The fitting was cast iron, which should have never been installed into the loop because of the potential for rust formation. It was likely installed because it was on hand in the lab at the time. Regardless of why it was chosen, it had to be replaced because it was leaking and crumbling to the touch. As stated in Appendix F, this work was done at the same time as the superheater changes were made. Figures G2 and G3 show other sections of pipe that were replaced at the same time as the rusted tee. The piping section of Figure G2 was severely discolored and had corrosion buildup from the failed rope heaters wound around it and thus needed to be replaced.



Figure G2: Corroded steam supply line upstream of the test section that was replaced when the superheater system was replaced.

Figure G3 shows a steam pressure regulator that was installed when the loop was initially built. The regulator was no longer in use and imparted a significant pressure drop (~ 8 psi), meaning the steam boiler had to be raised to a higher temperature to compensate. The regulator, and its ancillary piping were removed in Spring 2024 when the superheater changes described in Appendix F were made.

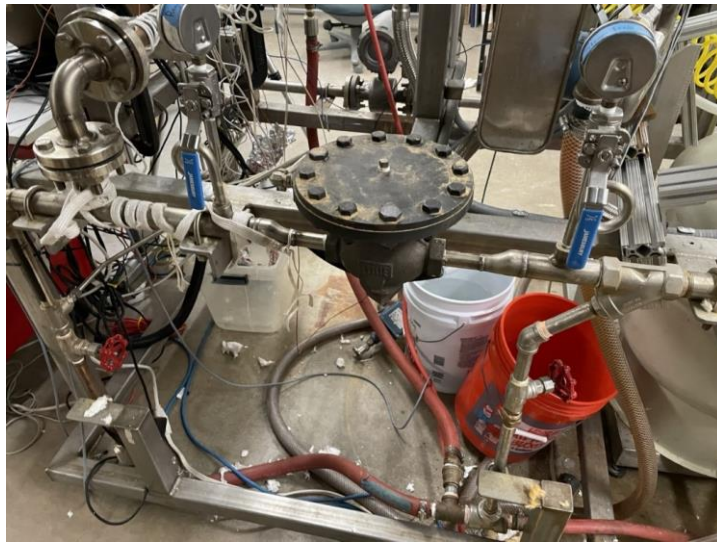


Figure G3: Cast iron steam pressure regulator installed up stream of the superheating section of pipe. Without a compressed air line, it served no purpose and was removed.

After removing the three major sections of pipe, replacements were made with the help of Hydrothermal's design engineering team. Hydrothermal provided sections of welded pipe with flange fittings and a pipe union to easy installation. Dimensions for piping from the removed pressure regulator to the front of the loop (to be under the test section, but not make the 90° bend upward) were given to Hydrothermal. We sourced the NPT fittings from the largest tee shown in Figure G4 up to the test section. In order to get the correct spacing to meet the bottom of the test section, a reducing bushing was used instead of a larger reducer. Multiple fully threaded pipe lengths were ordered and installed in a trial-and-error fashion.

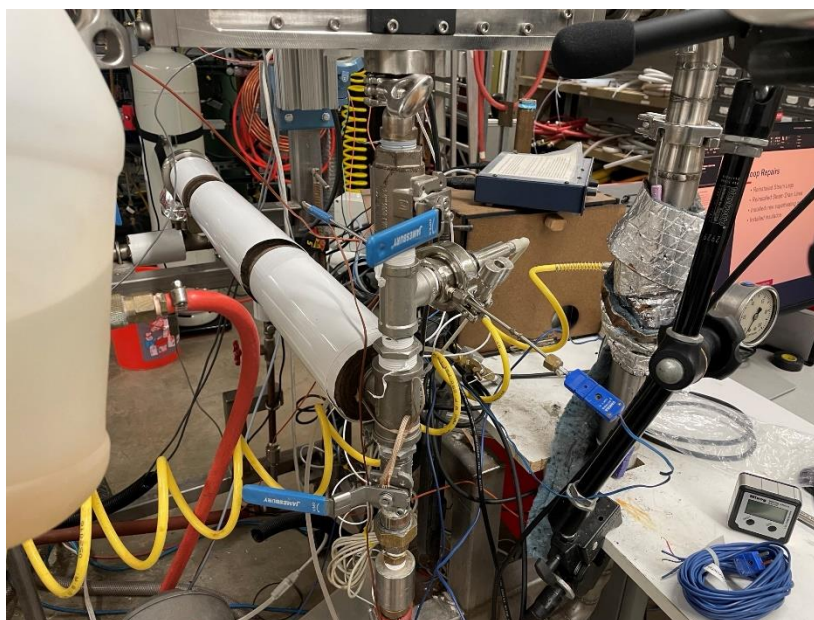


Figure G4: The updated front of the loop just below the test section as of October 2024. All fittings are exclusively 316 stainless steel for rust and corrosion resistance.

The new sections of pipe for the superheated section and the now removed pressure regulator are shown in Figures G5 and G6, respectively. Bulk vinyl faced pipe insulation and plastic pipe insulation sheathing was sourced from Hydrothermal. Each section was cut in the lab to allow gaps for the pipe supports. This change to preformed pipe insulation rather than the bulk insulation allows for much easier access for future maintenance and upgrades.

The process of replacing these plumbing changes took approximately three months, meaning there was no testing that could be carried out in the time frame. This should be a warning to future users of the test loop to avoid cast iron fittings as they will eventually rust and leak.

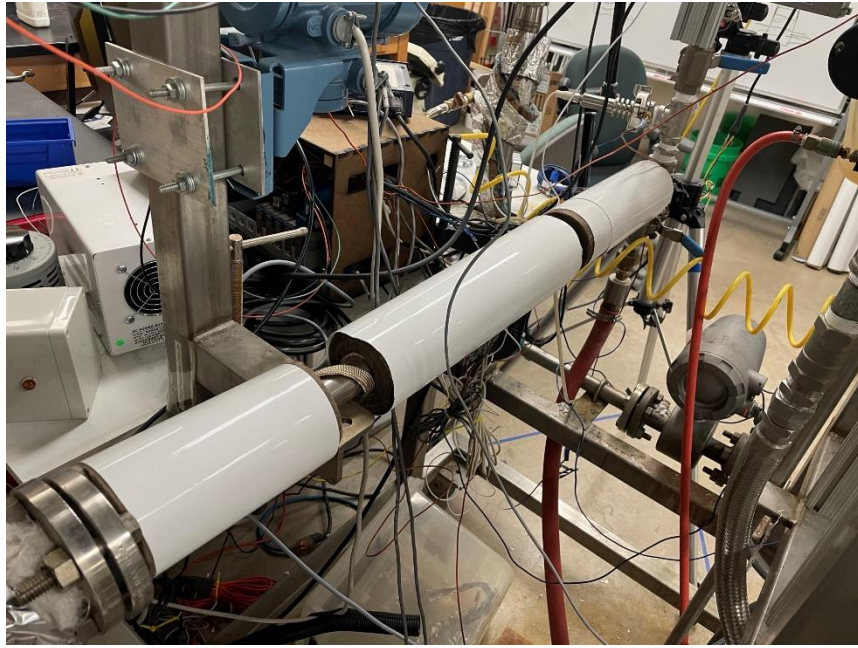


Figure G5: Insulated superheated section of new welded stainless-steel piping.



Figure G6: Back section of steam supply line after removing steam pressure regulator and replacing with new stainless-steel piping.

Appendix H: Data Organization

This section explains how to analyze data with the MATLAB scripts and Excel spreadsheet as of December 2024. All relevant files for data analysis are saved in the MFVAL drive at “X:\Steam Injection\Matlab Files\backlighting image processing 2023-06-26”. The three main files for data analysis are “StudyAnalysis.m”, “AnalysisFinal.m”, and “NozzleRegimeData.xlsx”. Both MATLAB codes pull information from the excel sheet, so it is important to fill out the spreadsheet during data collection. Think of “NozzleRegimeData.xlsx” as a lookup table for basic test information such as conditions and nozzle name that the MATLAB codes can then use to find the corresponding process data.

H.1 How to use NozzleRegimeData Excel Sheet

The “NozzleRegimeData.xlsx” is intended to be filled out before and during data collection for a nozzle test. Most data stored in the excel sheet is simple test information including process set points and the file directory for the corresponding test and ambient data. This excel sheet is organized so that each row has all the relevant info for one test and the columns are the various parameters read by the MATLAB scripts. The first column is a counter for naming the test. This is necessary because nozzle test names, saved in column B, can be identical given their naming convention (see Appendix A). For example, if doing a repeatability study where one nozzle at one pressure ratio is tested multiple times in one day they would have the same test name, but different “Test Numbers” based on the order that data was collected. Column C has the nozzle name based on the Test Name naming convention (see Appendix A), but deals only with the geometry, manufacturing, and orientation (if applicable) of the nozzle.

Columns D through O contain the manually classified flow regimes. Each column corresponds to one of the twelve temperatures that we take data at. As of December 2024, only four flow regimes are used: stable, condensation oscillation, transition, unstable (see Chapter 2.3 for description). Numbers 1 through 4 are then used to convey the regime in these columns with 1 being stable and 4 being unstable. A rule is set up to color code these cells as the regime number is entered to easily gauge a flow regime map. This section is easiest to fill out during data collection between temperature points as there is ample waiting time.

	A	B	C	D	E	F	G	H	I	J	K	L	M	N	O	P	Q	
1	Test Number	Test name	Nozzle name	Apparent regime at 25 [C]	30 [C]	35 [C]	40 [C]	45 [C]	50 [C]	55 [C]	60 [C]	65 [C]	70 [C]	75 [C]	80 [C]	Data Drive	Folder name	
264	Test263	1SE06515DPARA092524PRO46	1SE 0.065 ID 1.5D PARA	2	2	2	2	2	2	3	3	4	4	4	4	E:\	\\1SE06515DPARA092524PRO46\	1SE0651
265	Test264	1SE06515DPARA092724PRO58	1SE 0.065 ID 1.5D PARA	2	2	2	2	3	3	4	4	4	4	4	4	E:\	\\1SE06515DPARA092724PRO58\	1SE0651
266	Test265	1SE06535DPARA100924PRO46	1SE 0.065 ID 3.5D PARA	2	2	2	2	2	3	3	3	4	4	4	4	E:\	\\1SE06535DPARA100924PRO46\	1SE0653
267	Test266	1SE06535DPARA101624PRO58	1SE 0.065 ID 3.5D PARA	2	2	2	2	3	3	3	4	4	4	4	4	E:\	\\1SE06535DPARA101624PRO58\	1SE0653
268	Test267	1SE06525DPARA102424PRO46	1SE 0.065 ID 2.5D PARA	2	2	2	2	2	2	2	3	3	4	4	4	E:\	\\1SE06525DPARA102424PRO46\	1SE0652
269	Test268	1SE06525DPARA102424PRO58	1SE 0.065 ID 2.5D PARA	2	2	2	2	3	3	4	4	4	4	4	4	E:\	\\1SE06525DPARA102424PRO58\	1SE0652
270	Test269	1SE0651DNEW111524PRO46	1SE 0.065 ID NEW	1	1	1	1	1	2	2	2	3	3	4	4	E:\	\\1SE0651DNEW111524PRO46\	1SE0651
271	Test270	1SE0651DNEW111524PRO58	1SE 0.065 ID NEW	2	2	2	2	3	3	3	3	3	3	4	4	E:\	\\1SE0651DNEW111524PRO58\	1SE0651
272	Test271	1SE0801DNEW112224PRO46	1SE 0.080 ID NEW	2	2	2			2	2	3	4	4	4	4	E:\	\\1SE0801DNEW112224PRO46\	1SE0801
273	Test272	1SE0801DNEW112224PRO58	1SE 0.080 ID NEW	2	2	2	2	3	3			4	4	4	4	E:\	\\1SE0801DNEW112224PRO58\	1SE0801
274	Test273	1SE0801DNEW112524PRO46	1SE 0.080 ID NEW	1	2	2	2	2	2	2	2	3	4	4	4	E:\	\\1SE0801DNEW112524PRO46\	1SE0801
275	Test274	1SE0801DNEW112524PRO58	1SE 0.080 ID NEW	2	2	2	2	2	3	3	3	3	4	4	4	E:\	\\1SE0801DNEW112524PRO58\	1SE0801
276	Test275	1SE08015DPARA120424PRO46	1SE 0.080 ID 1.5D PARA	2	2	2	2					3				E:\	\\1SE08015DPARA120424PRO46\	1SE0801
277	Test276	1SE08015DPARA120624PRO58	1SE 0.080 ID 1.5D PARA	2	2	2	2	2	2	3	3	4	4	4	4	E:\	\\1SE08015DPARA120624PRO58\	1SE0801
278	Test277	1SE08025DPARA120924PRO58	1SE 0.080 ID 2.5D PARA													E:\	\\1SE08025DPARA120924PRO58\	1SE0802
279	Test278																	
280	Test279																	
281	Test280																	

Figure H1: Sample columns A to Q from the excel sheet.

Columns P through O shown in Figures H1 and H2 are for identification of the file directory where the corresponding test data is saved. Columns P and S are for naming the drive where the test data and ambient data are saved, respectively. Next, columns Q and T are for finding the folder in which data is saved for the test and ambient data. Last, columns R and U have the file prefix which every file within the directories of Q and T begin with.

Columns V through X contain the target steam pressure, water pressure, and water volume flow rate. Note that for the pressure ratio of 0.58, we target a water pressure of 34.4 psi, but you must enter a whole number in these cells otherwise the MATLAB scripts throw errors, so we usually round down to 34 psi. After taking the reference image (Appendix A.8) and calibrating what the pixel to inch conversion is, the normalization factor can be entered into column Y. This

cell is not currently used, but the framework exists for it to be implemented into an image processing algorithm.

	R	S	T	U	V	W	X	Y	Z
1	File Prefix	Ambient Drive	Ambient file name	Ambient File Prefix	Steam Pressure [psig]	Water pressure [psig]	Volume flow rate [ga/min]	video normalization factor [pixels/inch]	Nozzle Diameter
264	1SE0651SDPARA092524PR046	E:	\\AMB092524\	AMB092524	70	25	15	370	
265	1SE0651SDPARA092724PR058	E:	\\AMB092724\	AMB092724	70	34	15		
266	1SE0653SDPARA100924PR046	E:	\\AMB100924\	AMB100924	70	25	15		
267	1SE0653SDPARA101624PR058	E:	\\AMB101624\	AMB101624	70	34	15		
268	1SE0652SDPARA102424PR046	E:	\\AMB102424\	AMB102424	70	25	15		
269	1SE0652SDPARA102424PR058	E:	\\AMB102424\	AMB102424	70	34	15		
270	1SE065IDNEW111524PR046	E:	\\AMB111524\	AMB111524	70	25	15		
271	1SE065IDNEW111524PR058	E:	\\AMB111524\	AMB111524	70	34	15		
272	1SE080IDNEW112224PR046	E:	\\AMB112224\	AMB112224	70	25	15		
273	1SE080IDNEW112224PR058	E:	\\AMB112224\	AMB112224	70	34	15		
274	1SE080IDNEW112524PR046	E:	\\AMB112524\	AMB112524	70	25	15		
275	1SE080IDNEW112524PR058	E:	\\AMB112524\	AMB112524	70	34	15		
276	1SE0801SDPARA120424PR046	E:	\\AMB120424\	AMB120424	70	25	15		
277	1SE0801SDPARA120624PR058	E:	\\AMB120624\	AMB120624	70	34	15		
278	1SE0802SDPARA120924PR058	E:	\\AMB120924\	AMB120924	70	34	15		
279									
280									
281									
282									
283									
284									

Figure H2: Sample columns R to Z from the excel sheet.

Column Z is for the nozzle diameter in inches and is also not currently used in the MATLAB scripts. Information entered column AA is used as the legend entry when plotting in the StudyAnalysis MATLAB script. Finally, column AB has space for notes and is not used in the code. After entering information into each of these cells, the spreadsheet needs to be saved before it can be used by MATLAB.

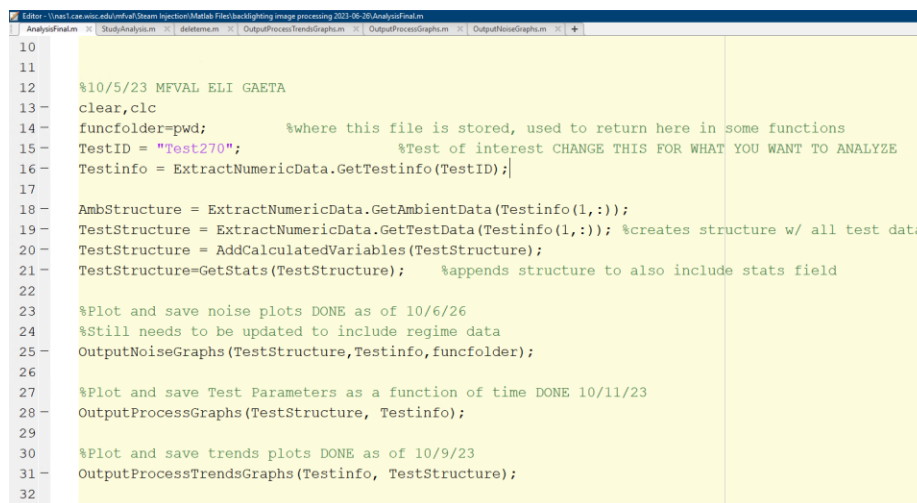
	X	Y	Z	AA	AB
1	Volume flow rate [ga/min]	video normalization factor [pixels/inch]	Nozzle Diameter [in]	Plot Name	Notes
264	15	370		0.065 1.5D 0.065 = 09/25/24	
265	15			0.065 1.5D 0.065 = 09/27/24	drained bladder tank after 65
266	15			0.065 3.5D 0.065 = 10/09/24	flow regimes around 65 are very different
267	15			0.065 3.5D 0.065 = 10/16/24	
268	15			0.065 2.5D 0.065 = 10/24/24	Changed steam thermocouple
269	15			0.065 2.5D 0.065 = 10/24/24	Regime based off of back plume
270	15			0.065 0.065 NEW EDM 11/11	New 0.065 nozzle/after superheating issues/jump in superheat from 40 to 70 degrees
271	15			0.065 0.065 NEW EDM 11/15/24	
272	15			0.08 0.08 NEW EDM 11/22	Flow was not completely deaerated
273	15			0.08 0.08 NEW EDM 11/22	Flow was not completely deaerated
274	15			0.08 0.08 NEW EDM 11/25/24	
275	15			0.08 0.08 NEW EDM 11/25/24	
276	15			0.08 1.5D 0.080 = 12/04/24	
277	15			0.08 1.5D 0.080 = 12/06/24	Chirping started at 75
278	15			0.08 2.5D 0.080 = 12/09/24	
279					
280					
281					
282					
283					
284					
285					
286					
287					

Figure H3: Sample columns X to AB from the excel sheet.

H.2 How to use AnalysisFinal.m

“AnalysisFinal.m” is a MATLAB code designed to output process and noise (dBa and FFTs graphs for each temperature and trend plots across the whole test. It is not a tool to output comparison plots between nozzles but is used to quickly evaluate the results from a single nozzle. The code has been commented and has custom functions that future users can edit for their needs.

The central working principle of the code is to use structure variables to load in and store all relevant data from the NozzleRegimeData Excel sheet, and csv files from testing. To analyze any data set, the only thing the user needs to change is the variable TestID to be a string of the test of interest as in Figure H4.



```

10
11
12 %10/5/23 MFVAL ELI GAETA
13 clear,clc
14 funcfolder=pwd; %where this file is stored, used to return here in some functions
15 TestID = "Test270"; %Test of interest CHANGE THIS FOR WHAT YOU WANT TO ANALYZE
16 Testinfo = ExtractNumericData.GetTestinfo(TestID);
17
18 AmbStructure = ExtractNumericData.GetAmbientData(Testinfo(1,:));
19 TestStructure = ExtractNumericData.GetTestData(Testinfo(1,:)); %creates structure w/ all test data
20 TestStructure = AddCalculatedVariables(TestStructure);
21 TestStructure=GetStats(TestStructure); %appends structure to also include stats field
22
23 %Plot and save noise plots DONE as of 10/6/26
24 %Still needs to be updated to include regime data
25 OutputNoiseGraphs(TestStructure,Testinfo,funcfolder);
26
27 %Plot and save Test Parameters as a function of time DONE 10/11/23
28 OutputProcessGraphs(TestStructure, Testinfo);
29
30 %Plot and save trends plots DONE as of 10/9/23
31 OutputProcessTrendsGraphs(Testinfo, TestStructure);
32

```

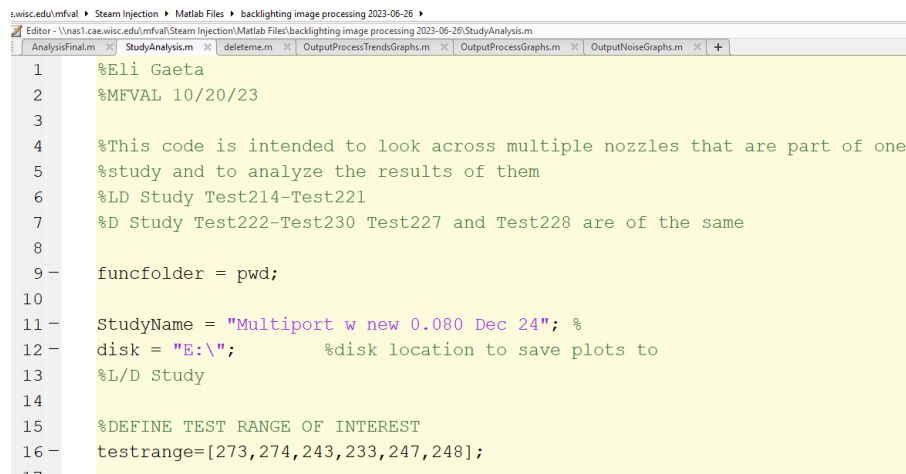
Figure H4: Code snippet from AnalysisFinal.m.

The functions called in Figure H4 are all saved in the same root directory as AnalysisFinal.m. These functions pull data from the Excel sheet to find testing data and fill out two structure variables AmbStructure and TestStructure. A function then calculates the mean, max, min, and standard deviation and appends them to the TestStructure variable. The “Output__Graphs” functions create plots for noise, process parameter at each temperature, and

process parameter trends and then saves them to the file directory of the whatever the “TestID” number is. Plots are all saved as both a .fig file and a .png so that they can be easily edited before printing again.

H.3 How to use StudyAnalysis.m

The purpose of the StudyAnalysis code is to compare multiple nozzles from a set of a study via plot. In general, this code works nearly identical to the AnalysisFinal code by utilizing structure variables to save test information and process data. Only trends plots are generated, meaning plots where the x-axes are temperature over the course of a test. All process parameters are plotted as well as noise level and FFT’s. Due to multiple tests being pulled, a new file directory needs to be created to save the plots as both .fig and .png to. This is what the variable StudyName in Figure H5 is for. It should be named appropriately based on the set of nozzles being compared. The local disk to save these plots is identified by the variable “disk”. The only other variable that must be specified by the user is an array variable to identify which tests should be pulled from the Excel spreadsheet, named “testrange”.



```

1      %Eli Gaeta
2      %MFVAL 10/20/23
3
4      %This code is intended to look across multiple nozzles that are part of one
5      %study and to analyze the results of them
6      %LD Study Test214-Test221
7      %D Study Test222-Test230 Test227 and Test228 are of the same
8
9      funcfolder = pwd;
10
11     StudyName = "Multiport w new 0.080 Dec 24"; %
12     disk = "E:\";           %disk location to save plots to
13     %L/D Study
14
15     %DEFINE TEST RANGE OF INTEREST
16     testrange=[273,274,243,233,247,248];
17

```

Figure H5: Code snippet from StudyAnalysis on the parts the user must edit before running.

After these three variables have been set, the user can then run the code. Two pop-up windows will then appear as shown in Figure H6. Figure H6a prompts the user whether data needs to be loaded into the TestStructure variable because this is the section of the code with the longest run time ~5 minutes. Unless the code was previously run the user should select “Yes” to this question. The second question in Figure H6b asks whether the user would like temperature error bars for each process parameter. These are helpful for understanding if the data points were at steady state with regard to test section temperature.

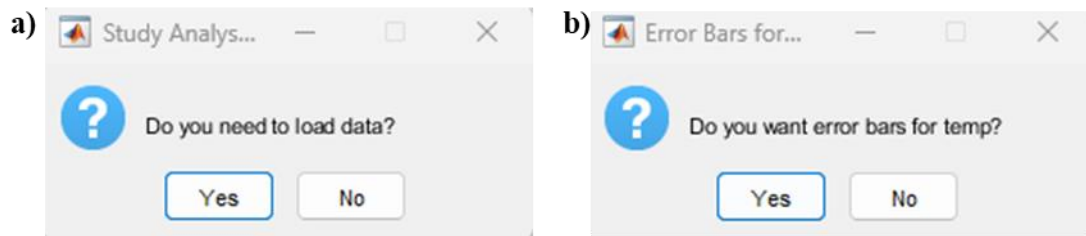


Figure H6: a) First pop up window after running StudyAnalysis.m asking if the user would like to load the data into the workspace. b) Second pop up window asking for input if x-error bars should be plotted.

After both prompts are answered, the code will begin to load data (if selected) and then proceed to create figures and save them. Each of the plots generated have error bars for the y axis variable that they are plotted against. These error bars are the range of values measured over the sampling period (i.e. the max and min) and not the standard deviation. This is most relevant for the noise level plots due to the transition region having a wide range of noise values because it has both condensation oscillation and unstable characteristics.